

# Role of thermal intensity on operational characteristics of ultra-low emission colorless distributed combustion



Vaibhav K. Arghode, Ashwani K. Gupta \*

Department of Mechanical Engineering, University of Maryland, College Park, MD 20742, USA

## HIGHLIGHTS

- Sequential development of high intensity CDC combustor from 5 to 453 MW/m<sup>3</sup> atm.
- Ultra low NO and CO demonstrated at thermal intensity of 340 MW/m<sup>3</sup> atm.
- Proper positioning of reaction zone is critical for low NO and CO emission.
- Residence time distribution governs CO emissions at same thermal intensity.
- Enhanced mixing in cross flow with low NO emission.

## ARTICLE INFO

### Article history:

Received 28 March 2013

Received in revised form 15 June 2013

Accepted 19 June 2013

Available online 22 July 2013

### Keywords:

Colorless distributed combustion

High intensity combustion

Ultra low emission and high performance

Novel non-premixed and premixed combustion

## ABSTRACT

This paper examines the development of ultra-low emission colorless distributed combustion (CDC) for gas turbines, operating at thermal intensity in the range of 5–453 MW/m<sup>3</sup> atm. Higher thermal intensity combustors are desirable for increased performance with minimal increase in hardware costs in terms of both weight and volume of gas turbine combustors. Most land based gas turbine combustors operate at thermal intensity of about 15 MW/m<sup>3</sup> atm but operation at higher intensity can provide increased performance. Design of high thermal intensity CDC combustor requires control of critical parameters, such as gas recirculation, fuel/oxidizer mixing, air preheats, and residence time distribution characteristics via proper selection of different air and fuel injection configurations to achieve desirable combustion characteristics. Initially, various flow field configurations were investigated at a low thermal intensity of 5 MW/m<sup>3</sup> atm. This effort was followed by investigations at higher thermal intensity ranges of 20–40 MW/m<sup>3</sup> atm by reducing the combustor volume for a forward flow configuration under more favorable novel non-premixed conditions. Further investigations were performed for a simpler combustor having single injection ports for air and fuel with detailed investigation of various flow field configurations performed at a thermal intensity of 28 MW/m<sup>3</sup> atm. Further reduction in combustion volume resulted in thermal intensity of 57 MW/m<sup>3</sup> atm. For the flow configurations investigated, reverse cross-flow configuration was found to give more favorable results with air injected from exit end and fuel injected in a cross-flow direction to the air flow. This reverse cross-flow geometry was investigated in detail by further reducing the combustor volume. Air injection diameter was increased to reduce the pressure drop across the combustor. The combustor was investigated at thermal intensity in the range of 53–85 MW/m<sup>3</sup> atm. This geometry resulted in 4 ppm NO emission and CO emissions of about 27 ppm under novel non-premixed flow conditions at thermal intensity of 53 MW/m<sup>3</sup> atm. The pressure drop at this operational point was less than 5% to meet the conventional combustor requirements. Further reduction in combustor volume resulted in very high thermal intensity in the range of 156–198 MW/m<sup>3</sup> atm and at the most desirable operational point NO and CO emissions were 8 ppm and 82 ppm, respectively under novel non-premixed mode at a thermal intensity of 170 MW/m<sup>3</sup> atm. Even further reduction in combustor volume resulted in combustor operation at ultra-high thermal intensity of 283–453 MW/m<sup>3</sup> atm and at the desirable operating point the NO and CO emissions were 4 ppm and 115 ppm respectively at a thermal intensity of 340 MW/m<sup>3</sup> atm. The sequential efforts reveal the possibility of significantly increasing the thermal intensity while still achieving desirable emission levels.

© 2013 Elsevier Ltd. All rights reserved.

\* Corresponding author. Tel.: +1 301 405 5276; fax: +1 301 314 9477.

E-mail address: [akgupta@umd.edu](mailto:akgupta@umd.edu) (A.K. Gupta).

**Nomenclature**

A	air	R	reverse flow (air injection from opposite side of combustor exit)
B	burned gases	S	fuel injection from same side of air injection
C	cross flow	T	temperature
C	tracer exit mass fraction	FO	air injection opposite to combustor exit, fuel injection opposite to air injection
CDC	colorless distributed combustion	FP	air and fuel premixed, mixture injection opposite to combustor exit
CFD	computational fluid dynamics	FS	air injection opposite to combustor exit, fuel injection on same side of air injection
D	diluted fuel (fuel and burned gas mixture)	RO	air injection on same side of combustor exit, fuel injection on opposite of air injection
D	diameter of air injection	RC	air injection on same side of combustor exit, fuel injection in cross flow to air injection
D	diffusion mode	RP	air and fuel premixed, mixture injection on same side of combustor exit
D <sub>con</sub>	length scale of confinement	RS	air injection opposite to combustor exit, fuel injection on same side of air injection
F	fuel	Vi	inlet velocity
F	forward flow (air injection from same side of combustor exit)	Vx	axial velocity
HiTAC	high temperature air combustion	W	length scale of combustor
L	length scale of combustor	X	distance along the combustor length
m <sub>air</sub>	mass flow rate of air	$\tau_{mix}$	turbulent mixing time
m <sub>fuel</sub>	mass flow rate of fuel	$\tau_{ign}$	ignition delay time
m <sub>ox</sub>	mass flow rate of oxidizer		
m <sub>rec</sub>	mass flow rate of recirculated gases		
O	oxidizer (air and burned gas mixture)		
O	fuel injection from opposite side of air injection		
O <sub>2</sub>	oxygen concentration		
P	premixed mode (air and fuel premixed prior to injection in combustor)		
psr	perfectly stirred reactor		

**1. Background of low emission combustors**

Demonstration and industrial implementation of high temperature air combustion (HiTAC) technology has been successfully realized for furnace applications worldwide where the thermal intensity is very low (about 0.1–1 MW/m<sup>3</sup> atm) and large combustion volume is available to achieve stable combustion [1–14]. Higher thermal intensity of about 10 MW/m<sup>3</sup> atm for furnace application was investigated for a forward flow configuration where a frustum of a cone was placed inside the combustor to enhance gas recirculation [13,14]. This technology has been further investigated for application to high thermal intensity gas turbine combustion development and has been termed as colorless distributed combustion (CDC). Note that the state of the art gas turbine combustor for land based power generation systems operates at thermal intensity of about 15 MW/m<sup>3</sup> atm [15]. Investigation for gas turbine combustor operating on the concept of distributed combustion was performed in both forward flow configuration [16] and reverse flow configuration [17] at thermal intensity of 14 MW/m<sup>3</sup> atm and 20 MW/m<sup>3</sup> atm, respectively. These combustors were termed as flameless oxidation (FLOX) and stagnation point reverse flow (SPRF) combustors respectively. Both of these combustors provided ultra-low NO<sub>x</sub> of only about 1 ppm and CO emission of less than 10 ppm at desired operational point. Trapped vortex combustor technology, where fuel is injected in a vortex that is trapped between two plates placed in the combustion air flow to enhance flame stability, was investigated at thermal intensity of 20 MW/m<sup>3</sup> atm [18] and 25 MW/m<sup>3</sup> atm [19]. These combustors demonstrated exceptional lean operational limits of overall equivalence ratio even less than 0.2 due to flame stabilization in a small cavity associated with the trapped vortex. The mixture in the trapped vortex is generally rich so that the hot gases produced are highly reactive for ignition of mixture in the main

combustion chamber. It is recognized that gas turbine combustors operate at elevated pressures. Note that, generally thermal intensity is considered in units of “MW/m<sup>3</sup> atm” [20] to compare different combustors as this definition also accounts for elevated pressure operation of gas turbine combustors.

A small scale jet stirred reactor having length scale of less than 1 inch has been investigated for the effect of pressure and residence time on lean premixed combustion and this combustor operated at thermal intensity of 90 MW/m<sup>3</sup> atm [21]. Trapped vortex combustor operating at high thermal intensity of 144 MW/m<sup>3</sup> atm has been previously investigated [22]; however, very high NO<sub>x</sub> emission of about 52 ppm and high CO emission of about 520 ppm were reported. Generally, land based gas turbine combustors operate at thermal intensity in the range of 5–50 MW/m<sup>3</sup> atm [20]; however, higher thermal intensity is desirable to further enhance efficiency, reduce combustor volume and weight as well as reduce the hardware costs. Higher thermal intensity combustor is even more desirable for aircraft gas turbine engines where both weight as well as volume is premium.

Important factors that need to be considered in the design of a CDC combustor are shown schematically in Fig. 1. Higher thermal intensity will result in smaller volume of the combustor; see Fig. 1a. Some of the basic requirements to achieve reactions close to CDC are separation of air ('A') and fuel ('F') streams to avoid direct reaction between the combustion air and fuel and controlled entrainment of burned gases ('B') in the air stream to result in the formation of high temperature and reduced but controlled oxygen concentration in the oxidizer ('O'); see Fig. 1b. This is then followed by mixing of oxidizer with the fuel jet to result in spontaneous ignition of the fuel to provide distributed combustion reaction zone, see Fig. 1c. These requirements can be partially met with different configurations of fuel and air injection. Air can be injected from opposite end of the exit (herein called as

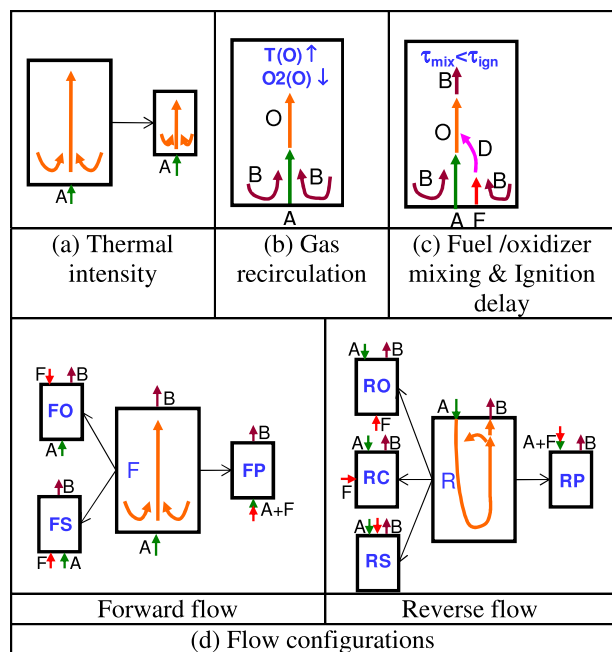


Fig. 1. Important factors for the design of CDC combustor.

forward flow configuration, 'F') or from the same end as exit (herein called as reverse flow configuration, 'R'). Fuel can be injected from same side of air injection ('S'), opposite side of air injection ('O'), in cross-flow ('C') or premixed with air prior to injection in the combustion chamber ('P'). Combination of these notations will give a specific flow configuration, for example, a combustor configuration in which air is injected from the same end as exit and fuel is injected from opposite side of air injection will be termed as 'RO', see Fig. 1d. The focus of this paper is to report sequential development of CDC technology for operation at thermal intensity range of 5–453 MW/m<sup>3</sup> atm for ultra-low emissions while investigating different flowfield configurations to achieve superior performance.

Fig. 2a shows the thermal intensities that have been investigated by various investigators as reported in the literature [1–9,11–19,22–23]. Thermal intensities up to 1 MW/m<sup>3</sup> atm are focused on furnace application and higher thermal intensities are focused on gas turbine combustion application. As observed from the figure very few studies have been reported at thermal intensity higher than 25 MW/m<sup>3</sup> atm. High thermal intensity of up to 144 MW/m<sup>3</sup> atm have been investigated previously for a trapped vortex combustor. It may be noted that the combustors reported in Fig. 2a operate in non-premixed mode wherein discrete injection of fuel and air is applied. The corresponding equivalence ratio is also included in the labels. The state of the art dry low NO<sub>x</sub> (DLN-2.6) gas turbine combustor is also included for comparison. DLN-2.6 combustor uses lean-premixed combustion technology and is fitted in a popular gas turbine GE-7FA. It operates at thermal intensity of about 15 MW/m<sup>3</sup> atm [15]. Fig. 2b shows the thermal intensities that have been investigated by the authors for a range of thermal intensity extending from 5 to 340 MW/m<sup>3</sup> atm. It may be noted that the highest thermal intensity combustor was investigated at thermal intensity range of 283–453 MW/m<sup>3</sup> atm and at the most desirable operational point the thermal intensity was 340 MW/m<sup>3</sup> atm [33]. The flowfield configuration notations are also included in the figure. For a given thermal intensity only the Favorably performing combustor has been included as many configurations of air and fuel injection have been examined by the authors at same thermal intensities. It may be noted that the combustors reported in Fig. 2b operate in novel non-premixed combustion modes.

Fig. 3a and c shows NO<sub>x</sub> and CO emission of combustors reported in the literature at the desirable operating condition. Fig. 3b and d shows NO and CO emissions of combustors reported by the authors. The state-of-the-art dry low NO<sub>x</sub> (DLN-2.6) gas turbine combustor produced less than 9 ppm of NO<sub>x</sub> as well as CO emissions [15]. Fig. 4a shows the length scale of combustors investigated by other authors in the literature and it may be noted that the combustors above 20 in. are generally intended for furnace application and smaller size combustors are intended for gas turbine combustion application. Combustor operating at low thermal intensity of 0.02 MW/m<sup>3</sup> atm had length scale of 246 in. [1] and combustor operating at high thermal intensity of 144 MW/m<sup>3</sup> atm had length scale of only 1.6 in. [22]. Fig. 4b shows the

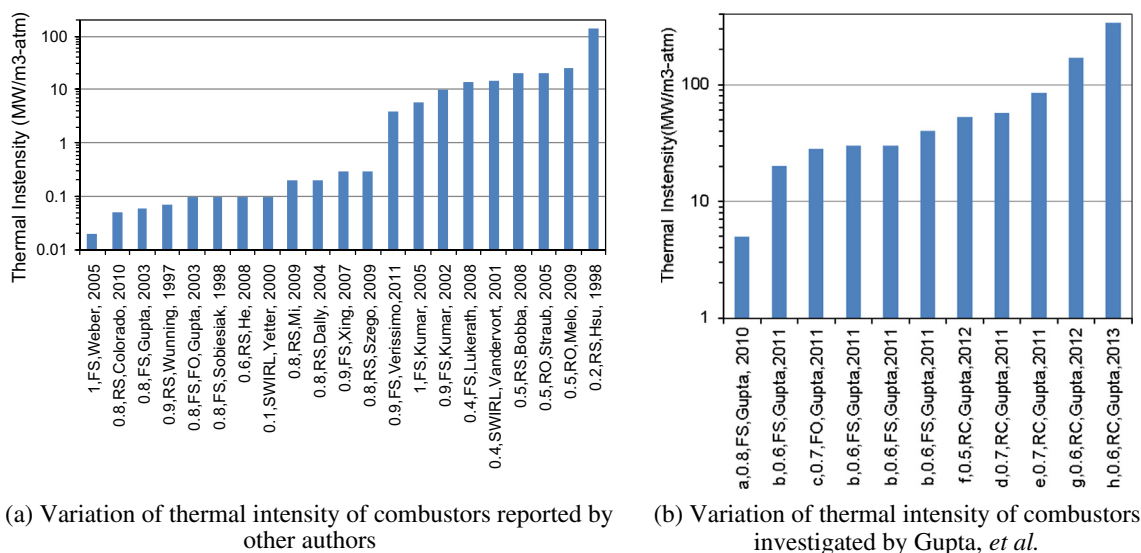
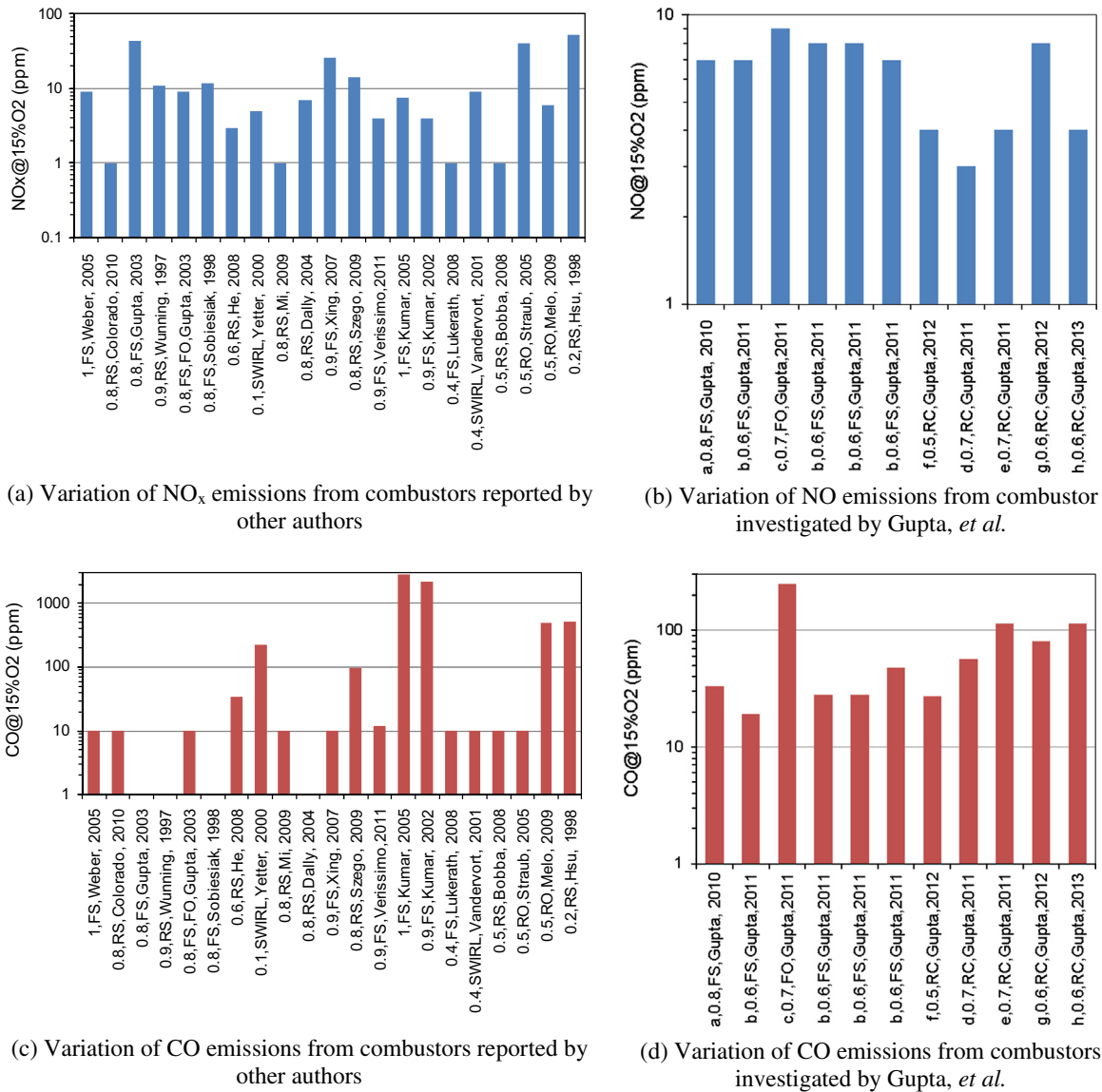


Fig. 2. Variation of thermal intensity for non-premixed combustors reported by (a) other authors (b) Gupta et al. for low emission combustors. a = [24], b = [25], c = [26], d = [27], e = [28], f = [29], g = [30], f = [31], g = [32], h = [33].



**Fig. 3.** Variation of NO<sub>x</sub>/CO emissions from non-premixed combustors reported by (a and c) other authors (b and d) Gupta et al. for low emission combustors.  $a = [24]$ ,  $b = [25]$ ,  $c = [26]$ ,  $d = [27]$ ,  $e = [28]$ ,  $f = [29]$ ,  $g = [30]$ ,  $f = [31]$ ,  $g = [32]$ ,  $h = [33]$ .

length scales investigated by the authors and it ranges from 9 in. for the combustor operating at thermal intensity of 5 MW/m<sup>3</sup> atm [24] down to 1.5 in. for combustor operating at thermal intensity of 340 MW/m<sup>3</sup> atm [33]. The state-of-the-art DLN-2.6 gas turbine combustor has a much larger length scale of about 60 in. [15].

A summary of other details of combustor performance operating in various configurations in both non-premixed and premixed modes reported in literature and investigated by the authors is given in Tables 1 and 2 respectively of the Appendix. The combustors are arranged in increasing order of thermal intensity.

## 2. Colorless distributed combustion and green combustion turbine

Colorless distributed combustion (CDC) has been investigated by the author's research group with the focus on development of

high thermal intensity, low emission combustors. CDC is based on the principle of high temperature air combustion (HiTAC) [3] that offers unique benefits in high intensity combustion. The name colorless is due to negligible visible emission from the flame as compared to conventional gas turbine combustion flames. The distributed combustion is from the distributed reaction zone in the entire combustion volume instead of a thin reaction flame front that promotes NO<sub>x</sub> formation in conventional combustion. Under some other conditions the flame produced is of green color so that this mode of combustion for high intensity gas turbine applications is called 'Green Combustion Turbine' and this will be discussed later. In both of the above cases the emissions are ultra-low with near uniform thermal field in the entire combustion zone so as to provide good pattern factor for gas turbine applications. The CDC conditions have demonstrated sound options to significantly reduce NO<sub>x</sub> and CO with no detectable emissions of hydrocarbons. In addition much enhanced pattern factor, high flame stability without using any flame stabilizer, low pressure drop and low

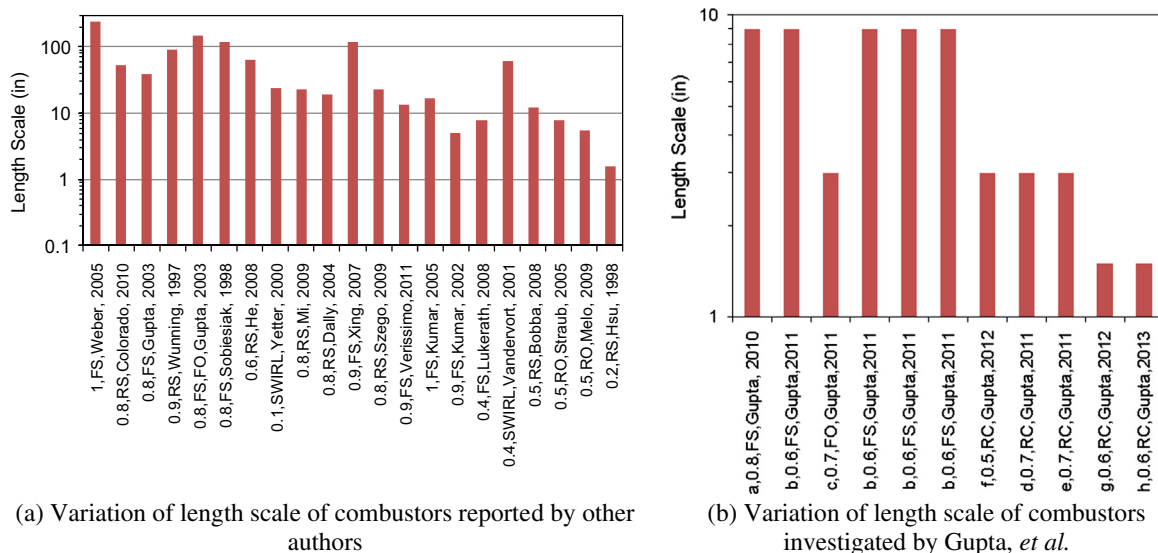


**Fig. 4.** Variation of length scale of non-premixed combustors reported by (a) other authors (b) Gupta et al. for low emission combustors.  $a = [24]$ ,  $b = [25]$ ,  $c = [26]$ ,  $d = [27]$ ,  $e = [28]$ ,  $f = [29]$ ,  $g = [30]$ ,  $f = [31]$ ,  $g = [32]$ ,  $h = [33]$ .

noise levels from the combustor was observed [24–33]. Due to uniform thermal field in the entire combustion zone (much improved pattern factor) the amounts of air cooling required to cool turbine blades is expected to be reduced which can result in improved efficiency and performance.

Distributed combustion is characterized by discrete and direct injection of air and fuel in a confined volume to avoid direct mixing and reaction of fuel and combustion air. Controlled hot product gas recirculation and novel injection schemes are required to provide fast fuel/oxidizer mixing at high reactants temperatures. This results in favorable distributed combustion conditions and simultaneously avoids stoichiometry variation that helps to eliminate the hot spot regions formed in traditional gas turbine combustors. High temperature air from the compressor is shown to be favorable for reducing CO emission while maintaining ultra-low  $\text{NO}_x$  emission levels and good pattern factor. Auto ignition of the fuel, as used in HiTAC technology, is much different to fully support the CDC operation. Focus here is on development of high and ultra-high thermal intensity CDC combustor for land based gas turbine application with greater efficiency and near zero emissions of  $\text{NO}_x$  and CO.

Advanced combustion technologies are required to meet stringent emission norms as well as to reduce costs of the combustion system. Colorless distributed combustion examined here demonstrates ultra-low emissions with very compact combustion volume (at high thermal intensity). Smaller volume will relate to significant savings in capital costs. Detailed fundamental understanding of distributed combustion is required to achieve improved mixing of the reactants prior to combustion leading to distributed reactions in the entire combustion volume with uniform thermal field. This will result in much improved pattern factor, less cooling air requirements for the turbine blades and significant increase in turbine blade life. Other challenge is to achieve distributed reactions coupled with low turbulence level which will result in very lower pressure drop across the combustor and hence increased efficiency. Detailed understanding of  $\text{NO}_x$  formations mechanisms under hot and diluted conditions is required so as to reduce  $\text{NO}_x$  from prompt and  $\text{N}_2\text{O}$  intermediate mechanisms apart from thermal mechanism. This will lead us to the goal of near zero  $\text{NO}_x$  emissions in future. Wider shear layer mixing regions (radially stretched) near the

air and fuel jets is required so as to distribute the reactions in larger volume as compared to thin reaction zones encountered in conventional gas turbine combustors. Advanced swirling distributed combustion can be investigated to achieve higher gas recirculation and intense mixing so as to achieve high residence time and complete combustion with near zero  $\text{NO}_x$  emissions.

Another revolutionary concept of ‘Green Combustion Turbine’ will be investigated in future with aim of near zero pollutant emissions. The visible emission from flame was observed to be shifted towards green due to dominance of  $\text{C}_2$  radical (swan band) under high temperature air combustion condition [34,35], especially with propane and heavier fuels, with reactions occurring at near uniform temperatures. With decrease in oxygen concentration the flame color was observed to change from yellow to blue to bluish green to green color and at very low oxygen concentration of less than 2% no color was observed and this was termed as ‘colorless combustion’. At lower oxygen concentration (<5%) green color flame was observed due to domination of  $\text{C}_2$  radical emission [34,35] and this is termed as “Green Combustion Turbine”. This green flame was observed to result in very low pollutant emissions and these specific conditions could be investigated to achieve ultra-low pollutant emissions for high thermal intensity combustors.

### 3. Background calculations for effect of thermal intensity

The main focus of this paper is on successful sequential development of high intensity gas turbine combustor by the authors with successive increase in thermal intensity that extend well into next generation of gas turbine combustors. Sample calculations are presented in this section to understand and unravel the effects of various important parameters, such as residence time and gas recirculation on thermal intensity and emissions from a combustor. Higher thermal intensity is desirable so that the same amount of heat could be released in a smaller combustor volume and this directly relates to reduced hardware costs. As an example, increase in thermal intensity from 5 to  $50 \text{ MW/m}^3 \text{ atm}$  would require a combustor having 1/10th volume as compared to the original combustor for the same heat load.



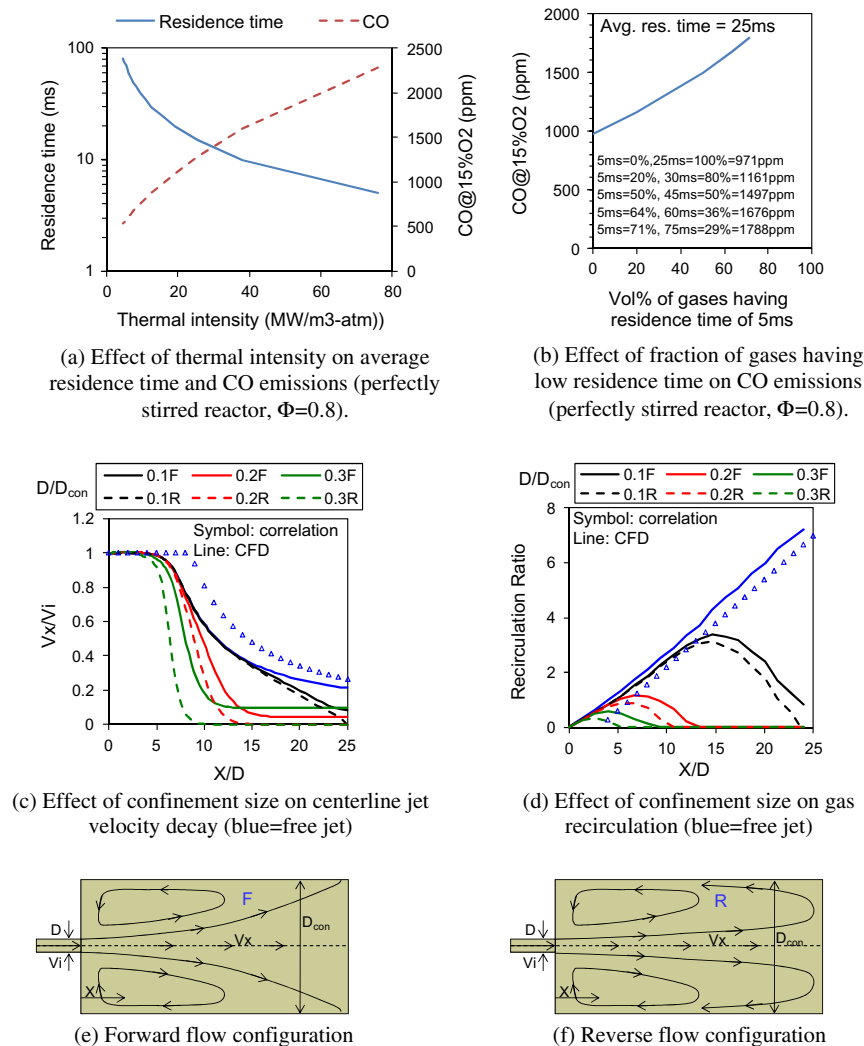


**Fig. 5.** (a) Effect of thermal intensity on residence time and CO emissions. (b) Effect of fraction of gases having low residence time on CO emissions. (c) Effect of confinement size on velocity decay. (d) Effect of confinement size on gas recirculation. (e) Schematic of forward flow configuration. (f) Schematic of reverse flow configuration.

Higher thermal intensity will result in lower residence time due to higher volume flow rate of air and fuel for the same thermal load. The effect of thermal intensity on residence time and CO emissions is shown in Fig. 5a. Chemical kinetic simulations for a perfectly stirred reactor model are performed using GRI-3.0 mechanism [36] at equivalence ratio of up to 0.8, inlet temperature of 300 K and pressure of 1 atm. Note that equivalence ratios of 0.8 are very high for current gas turbine combustors that operate at much lower equivalence ratios of 0.5 or less, however, the inlet air temperatures are higher due to compression. For these simulations commercial software code CHEMKIN was used. The oxidation of CO is a slow process in all combustion systems so that lower residence time will result in higher CO emission levels at the exit. The figure suggests that higher thermal intensity will correspond to lower residence time and hence it will result in higher CO emissions as shown in Fig. 5a. For example, thermal intensity of 5 MW/m<sup>3</sup> atm results in a residence time of 76 ms and thermal intensity of 75 MW/m<sup>3</sup> atm results in a residence time of 5 ms. This results in CO emission of about 2280 ppm at 75 MW/m<sup>3</sup> atm as compared to 550 ppm at 5 MW/m<sup>3</sup> atm. It may be noted that for higher pressure operation, the relation between residence time and thermal intensity will be same. At a given thermal intensity,

at higher pressures, one can burn more fuel (higher heat load); however on the other hand the velocities will be same as the gas density will increase linearly with pressure resulting in the same residence time. Hence it may be noted that thermal intensity is an indication of average residence time in a combustor. The calculation for CO levels for average residence time of 25 ms with different percentage of gases having low residence time is shown in Fig. 5b. From the figure it can be noted that if one has higher fraction of gases having low residence time, CO emissions will increase even though the average residence time is same of all the cases. For example, if we have all the gases having residence time of 25 ms the CO emission from perfectly stirred reactor will be 971 ppm. However, if 71 vol.% of gases has residence time of 5 ms and 29 vol.% of gases has residence time of 75 ms (giving 25 ms of average residence time) CO emission is 1788 ppm. Hence, with favorable residence time distribution, where one has minimal fraction of gases having low residence time, one can have higher conversion of CO and consequently lower CO emissions.

For the same heat load, to achieve higher thermal intensity a smaller confined volume will be required. With reduction in volume, the confinement effects are expected to dominate the flow field inside the combustor. To understand the effect of confinement

on gas flow and recirculation inside the combustor, CFD simulations were performed on an axisymmetric jet and results are shown in Fig. 5c and d. Two types of geometries were considered for the simulation. In the first geometry the air exits from the opposite end of air injection and this geometry is a representative of forward flow configuration (denoted as 'F', see Fig. 5e). In the other geometry, air exits the confinement from the same side of air injection and this geometry is representative of a reverse flow configuration (denoted as 'R', see Fig. 5f). Realizable  $k$ - $\epsilon$  model with standard wall functions were used to model turbulence with inlet turbulence intensity of 5%. Realizable  $k$ - $\epsilon$  model has been shown to provide more accurate prediction of profile and spreading of non-reacting round jets [37]. The inlet air velocity is 128 m/s and this corresponds to the examined heat load of 6.25 kW using methane as the fuel burning at equivalence ratio of 0.8. Note that this equivalence ratio is much higher than that used in conventional gas turbine engines. The conditions given above have been used here for various configurations investigated over a range of thermal intensities. Convergence was obtained when the residuals for all the variables were less than  $1\text{E-}04$ . Air at normal temperature and pressure was used as the working fluid. For these simulations commercial software FLUENT was used.

The results for centerline air jet velocity decay are shown in Fig. 5c. From the figure it can be observed that with smaller confinement size (higher  $D/D_{\text{con}}$  ratio, where  $D$  is the air injection diameter and  $D_{\text{con}}$  is the length scale of the confinement) the velocity decay is faster. It may also be observed that the jet velocity decay is faster for reverse flow configuration as compared to the forward flow configuration. The results for gas recirculation are presented in Fig. 5d. It may be noted that for smaller confinement volume, the maximum gas recirculation is limited by the confinement size. The gas recirculation increases along the length, reaches a peak value and then decreases. This also suggests that higher thermal intensity may pose problems on the stabilization of reactions as well as high temperature mixture preparation that is critical to achieve reactions in distributed combustion (CDC) mode. Reverse flow configuration results in slightly lower gas recirculation as compared to the forward flow configuration. It may be noted that for reverse flow configuration while calculating the

mass flow rate of the recirculated gases, the mass flow rate of injected air is subtracted from the total flow rate having the negative velocity as the mass flow rate of injected air has to reverse its direction of flow before exiting the combustor. The gas recirculation for free jet is slightly over predicted by the CFD simulations as compared to the correlation given in [38]. This requires further substantiation and validation using detailed experimental data.

At higher gas recirculation ratios the oxidizer (mixture of recirculated product gases and injected air) temperature will increase and the oxygen concentration will decrease. To obtain the values of oxidizer temperature and oxygen concentration, chemical kinetic simulation has been performed using the GRI 3.0 reaction mechanism [36] for an adiabatic well stirred reactor (at residence time = 100 ms) using methane as the fuel with both fuel and air entering the combustor at an inlet temperature of 300 K and overall equivalence ratio of 0.8. The product gas from the first reactor is mixed with air in the second reactor to form the oxidizer as shown in Fig. 6c. The ratio of mass flow rates in first reactor ( $m_{\text{rec}2}$ ) and the mass flow rate of air ( $m_{\text{air}2}$ ) in the second reactor will govern the recirculation ratio. The results of oxidizer temperature and oxygen concentration are presented in Fig. 6a and that of ignition delay times are presented in Fig. 6b. It can be observed that for recirculation ratio in the range of 2–3, the temperature of oxidizer is about 1530–1655 K and oxygen concentration is in the range of 9.4–8 vol.%. For spontaneous ignition of fuel and oxidizer mixture the ignition delay time should be well below the residence time in the combustor. For recirculation ratio of 3 the ignition delay time is about 1 ms. The results are compared with correlation for ignition delay time for methane combustion in air given in [39].

From these simple calculations it may be conjectured that increase in thermal intensity poses many challenges of reduced residence time, to possibility promote higher CO emissions as well as reduce gas recirculation which can pose problems of spontaneous ignition and flame stabilization.

In the present investigation, various flow field configurations for range of thermal intensities in the range of 5–453 MW/ $\text{m}^3 \text{ atm}$  has been reported and these results could be useful for designing gas turbine combustors operating on CDC technology. The results are specifically reported for combustors operating at

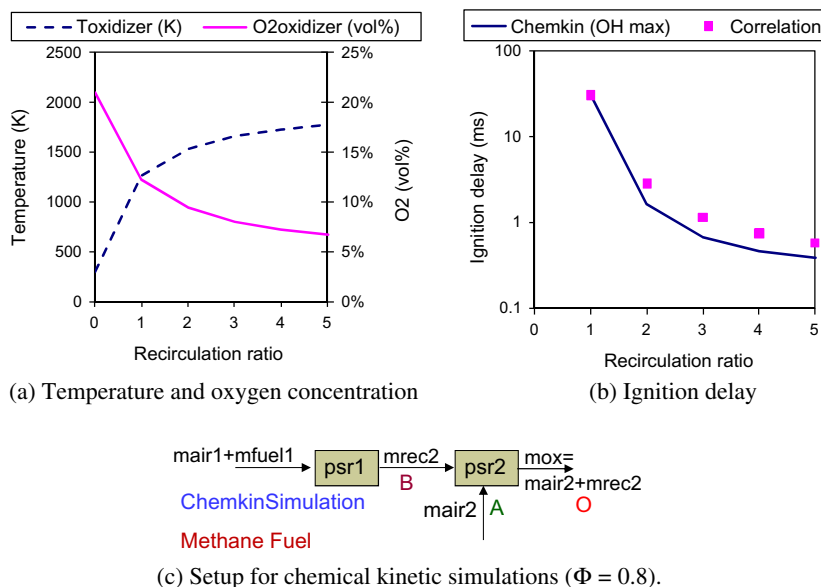
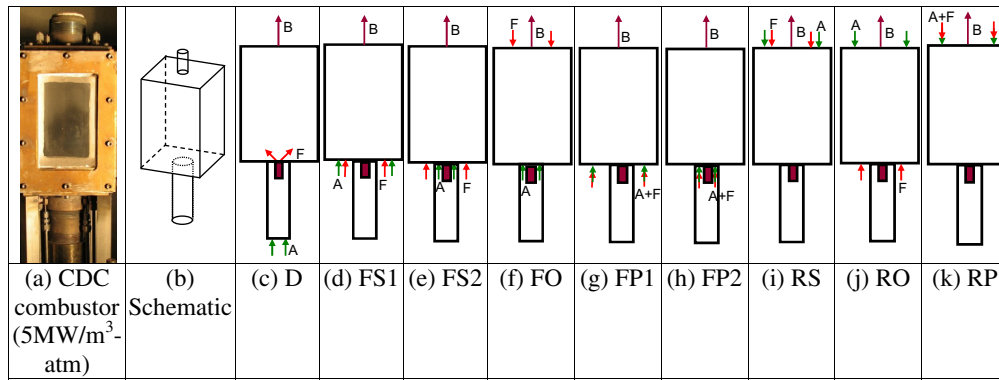


Fig. 6. (a) Effect of gas recirculation on temperature and oxygen concentration of oxidizer. (b) Effect of gas recirculation on ignition delay time. (c) Setup for chemical kinetic simulations.



**Fig. 7.** CDC combustor at thermal intensity of  $5 \text{ MW/m}^3 \text{ atm}$  (a) photograph, (b) schematic and (c–k) schematic diagrams of different geometries examined, heat load is 25 kW.

5, 20, 30, 40, 28, 53, 57, 85, 170 and  $340 \text{ MW/m}^3 \text{ atm}$ . The results are also summarized in Table 2 of the Appendix.

#### 4. Low thermal intensity combustor ( $5 \text{ MW/m}^3 \text{ atm}$ )

##### 4.1. Effect of flowfield configuration ( $5 \text{ MW/m}^3 \text{ atm}$ )

Initially a low thermal intensity combustor operating at  $5 \text{ MW/m}^3 \text{ atm}$  was designed and examined. This combustor had four air and four fuel injection ports with the desired flexibility to operate in various air and fuel injection configurations. A photograph of this combustor and different flow configurations investigated is shown in Fig. 7. Eight flow field configurations are reported that show the potential to achieve reactions in more favorable colorless distributed combustion (CDC) mode. These include five forward flow configurations ('FS1', 'FS2', 'FO', 'FP1', 'FP2') and three reverse flow configurations ('RS', 'RO', 'RP'). The combustor is started in diffusion flow mode ('D') and then transitioned to CDC mode. The combustor operates at heat load of 25 kW with methane as the fuel and air as oxidizer and four air and fuel injection ports were used. Both air and fuel were injected at ambient temperature and the combustor was operated at atmospheric pressure. In all the cases examined here, at different thermal intensities, no catalyst was used for the onset of or sustaining the combustion. Fuel injection velocity was 97 m/s, and air injection velocity was 128 m/s at rather high equivalence ratio of 0.8. Further details of the experimental conditions are provided elsewhere [24].

The results for NO and CO emissions at equivalence ratio of 0.8 are shown in Fig. 8. It can be observed that the novel premixed flow

mode ('FP1', 'FP2', 'RP') produced lowest NO levels (about 1 ppm). Lowest CO emission (about 5 ppm) was obtained for reverse flow configuration operating in the novel premixed mode ('RP'). This may be due to higher fraction of gases having higher residence time associated for this configuration as compared to other forward flow configurations ('FP1' and 'FP2') as the burned gases has to reverse the direction before exiting from the combustor. Amongst the novel non-premixed modes, configuration 'FS1' resulted in low NO (about 7 ppm) and low CO (about 33 ppm) emission levels. As the air injection port was shifted towards the combustor centerline ('FS2', 'FP2'), CO emissions increased significantly as compared to the configurations where air injection port was near the combustor walls ('FS1', 'FP1'). This may be due to higher fraction of gases having lower residence time for this configurations 'FS2' and 'FP2' due to faster escape of burned gases from the combustor exit which is located along centerline of the combustor. This highlights the importance of location of injection of the reactants into the combustor.

Numerical calculations of residence time distribution were performed for configurations 'FP1', 'FP2' and 'RP'. First a steady state solution of non-reacting (only air) flow field was obtained and then a tracer, having same property as that of air introduced from the air injection location, and the exit mass fraction is tracked with respect to time. Further details of numerical set-up and calculation of residence time can be found elsewhere [26,27]. Residence time calculations for the three novel premixed flow modes ('FP1', 'FP2' and 'RP') are shown in Fig. 9. Fig. 9a shows the exit mass fraction profile and Fig. 9b shows the residence time frequency distribution. The average residence time for the three cases is 589 ms for

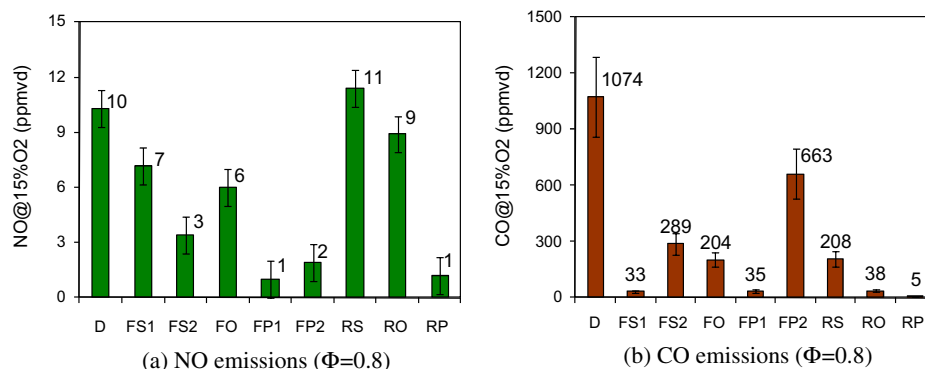


**Fig. 8.** (a) NO and (b) CO emissions of CDC combustor at thermal intensity of  $5 \text{ MW/m}^3 \text{ atm}$  and heat load of 25 kW, for different flow-field configurations.



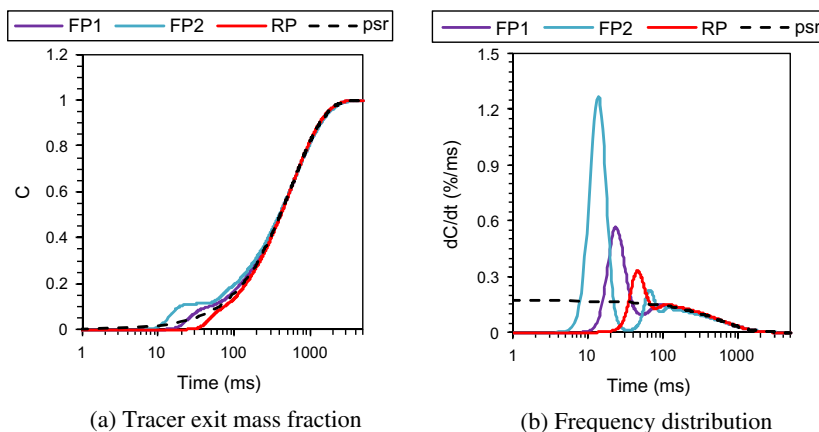


Fig. 9. (a) Tracer exit mass fraction and (b) frequency distribution for configurations FP1, FP2 and RP and its comparison with perfectly stirred reactor (psr).

'FP1', 588 ms for 'FP2', 590 ms for 'RP' and 585 ms for perfectly stirred reactor (psr). This suggests that the average residence time is very close to that for a perfectly stirred reactor irrespective of the flow configuration.

However, as observed from the frequency distribution, configuration 'FP1' has the highest fraction of tracer particles having low residence time, whereas configuration 'RP' has lowest fraction of tracer particles having low residence time. This could also be observed from early inception of tracer at the exit for configuration 'FP2' as compared to configuration 'RP'. From Fig. 5b we learn that for the case with higher fraction of gases having lower residence time can lead to overall high emission of CO in the exit gases even though the average residence time is same. Hence the residence time calculation suggests that the reverse flow configuration can result in lowest CO emissions for the present case. This further suggests that, location of air injection port which will result in higher residence time can result in lower CO emissions. The figure also suggests that enhanced performance as compared to perfectly stirred reactor could be achieved by selectively choosing the flow configurations, as perfectly stirred reactor has higher fraction of gases having very low residence time as compared to other flow configurations. These simple calculations also suggests that one can have benefit of favorable residence time distribution by tailoring the flow field by operating optimal configuration even though the average residence time is the same for different configurations for a given volume.

## 5. Medium thermal intensity combustor (20–60 MW/m<sup>3</sup> atm)

### 5.1. Combustor operation at 20–40 MW/m<sup>3</sup> atm

Previous investigation of combustor performance at thermal intensity of 5 MW/m<sup>3</sup> atm revealed that placing air injection port away from the combustor centerline for forward flow mode results in favorable residence time characteristics of gases in the combustor and that the configuration in novel non-premixed mode ('FS1') resulted in favorable emission characteristics. In the next step the thermal intensity of a forward flow configuration was increased to 20–40 MW/m<sup>3</sup> atm range by reducing the confinement size using three different diameter cylindrical quartz tubes. The configuration is similar to the forward flow configuration 'FS1' investigated previously wherein the air is injected near the combustor walls and fuel is injected near the combustor centerline from opposite end of the combustor (see Fig. 7d). The combustor was operated at heat load of 25 kW at normal temperature of air and fuel injection and at atmospheric pressure using four air and four fuel injection ports. Air injection velocity was varied from 146 to 205 m/s to result in the corresponding equivalence ratio variation from 0.7 to 0.5. Fuel injection velocity was 97 m/s. Further details of geometry and experimental conditions are provided elsewhere [25].

Fig. 10 shows the global flame images of conventional diffusion flame mode similar to configuration 'D' and non-premixed CDC mode similar to configuration 'FS1'. It can be observed that

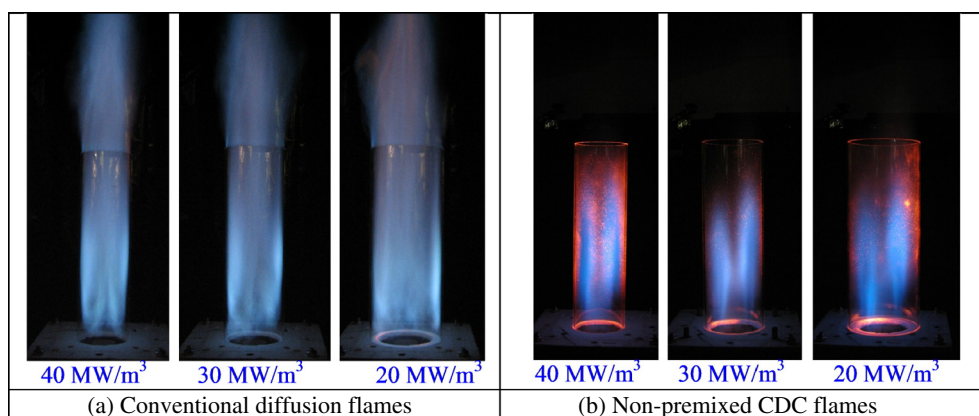


Fig. 10. Global flame images for (a) diffusion flames (D) and (b) non-premixed CDC flames (FS1), heat load is 25 kW.

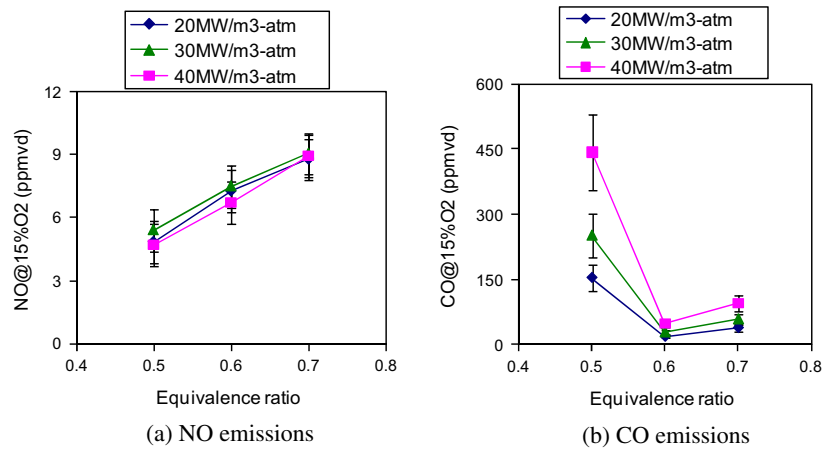


Fig. 11. (a) NO and (b) CO emissions of CDC combustor for forward flow configuration FS1 for effect of thermal intensity at heat load of 25 kW.

conventional diffusion flame could not be contained inside the confinement volume and hence it really does not represent high thermal intensity operation of combustor. However, the novel non-premixed CDC flames were observed to be confined inside the confinement volume resulting in thermal intensity range of 20–40 MW/m³ atm.

Fig. 11 shows the emissions of NO and CO for the effect of thermal intensity in the range of 20–40 MW/m³ atm for the forward flow configuration 'FS1'. It can be observed that for the range of thermal intensity investigated here the NO emissions are similar;

however, CO emissions increase significantly with increase in thermal intensity. This can be attributed to smaller residence time corresponding to higher thermal intensity case (see Fig. 5a). Furthermore reduction in confinement volume also results in reduction in gas recirculation as observed numerically, see Fig. 5b.

## 5.2. Combustor operation at 28 MW/m³ atm

Different flow field configurations at thermal intensity of 28 MW/m³ atm were investigated using a simplified geometry of

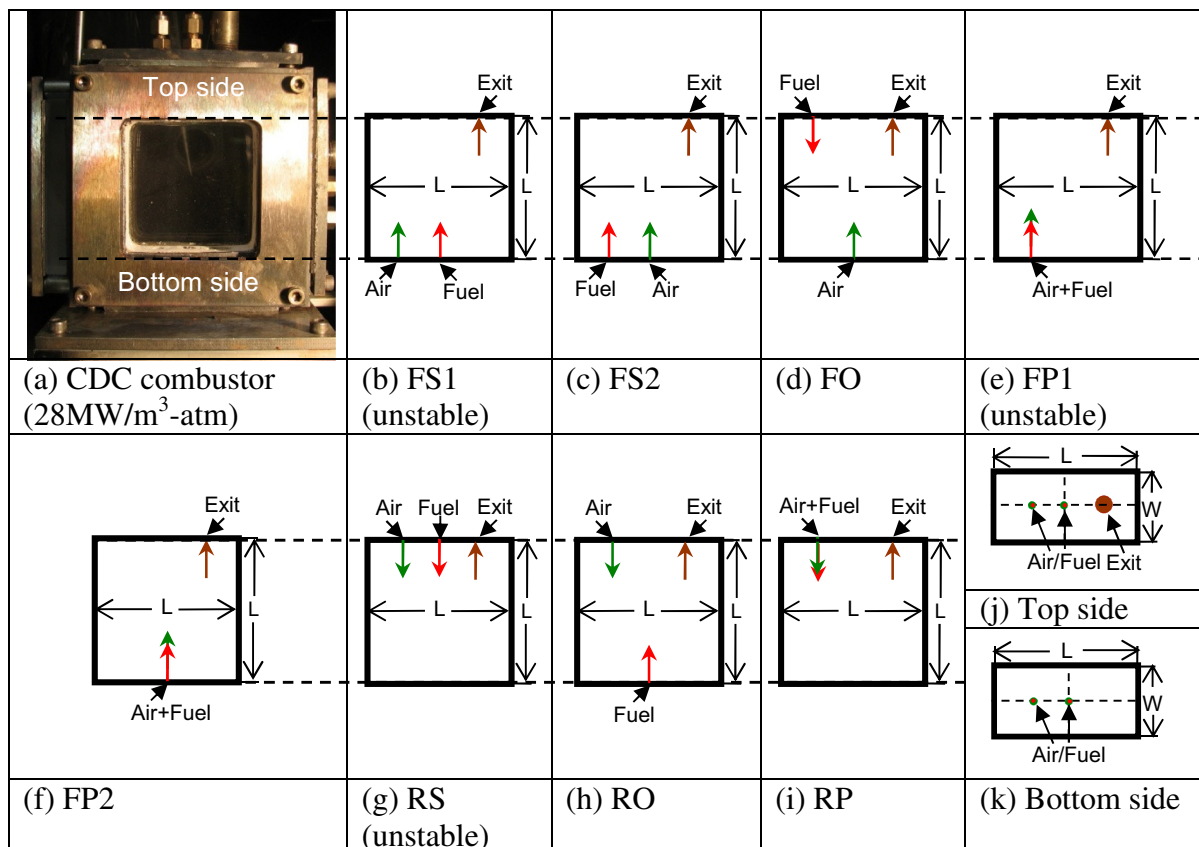


Fig. 12. CDC combustor (28 MW/m³ atm, 6.25 kW) (a) photograph and (b–k) schematic diagrams of different geometries examined.

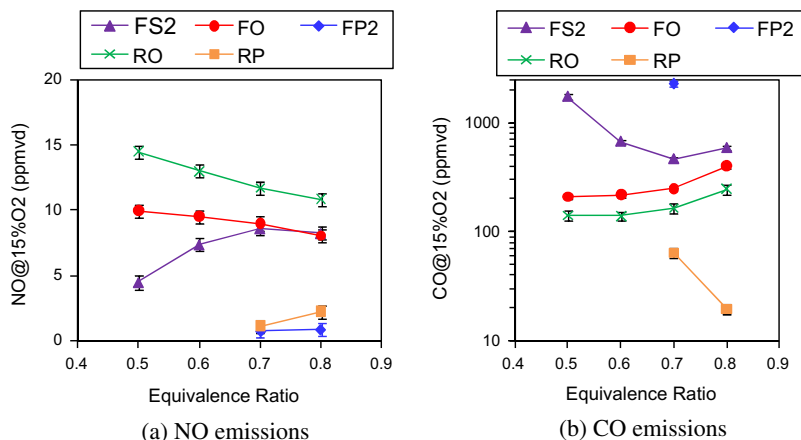


Fig. 13. (a) NO emissions and (b) CO emissions for the CDC combustor at thermal intensity of 28 MW/m<sup>3</sup> atm and heat load of 6.25 kW.

the combustor. Only single air and fuel injection ports were used as compared to four air and four fuel injection ports used previously. Different flow configurations including both forward and reverse flow were investigated. The heat load was fixed at 6.25 kW and air and fuel was injected at normal temperature and combustor operated at atmospheric pressure for all the cases. The fuel injection velocity was 97 m/s and air injection velocity varied from 128 to 205 m/s to provide the variation in equivalence ratio from 0.8 to 0.5, respectively. Further details of the experimental conditions are given elsewhere [26,27].

Similar to the forward and reverse flow configurations investigated for thermal intensity of 5 MW/m<sup>3</sup> atm (see Fig. 7), different configurations at higher thermal intensity of 28 MW/m<sup>3</sup> atm were investigated; see Fig. 12 for more details. Note that higher thermal intensity results in lower residence time and reduced recirculation of gases which subsequently pose problems of sustaining combustion and results in higher emissions of CO, see Fig. 5a. Configurations 'FS1', 'FP1' and 'RS' could not sustain combustion due to lower recirculation of gases as well as slower decay of fuel jet as observed numerically [26,27]. Hence experimental results for these cases are not presented. It may be noted that the configuration 'FS1' provided lower NO as well as lower CO emissions for the low thermal intensity case in the non-premixed mode, see Fig. 8. This suggests that the geometry has influence on combustion characteristics of different configurations and this factor needs to be considered while scaling CDC combustors.

Experimental results on the NO and CO emissions at thermal intensity of 28 MW/m<sup>3</sup> atm are shown in Fig. 13. The novel

premixed flow mode in both forward ('FP2') and reverse ('RP') flow configuration resulted in lowest NO levels (about 1 ppm); however CO emission was very high (about 2300 ppm) for the forward flow configuration but considerably low (about 50 ppm) for the reverse flow configuration. This further emphasize that the reverse flow configuration results in favorable residence time distribution and hence lower CO emission as compared to the forward flow configuration. This result is similar to that reported in Fig. 8 for lower thermal intensity combustor operating at thermal intensity of 5 MW/m<sup>3</sup> atm. It may also be noted that the increase in thermal intensity from 5 to 28 MW/m<sup>3</sup> atm increased the CO emissions considerably due to lower associated residence time for the high intensity combustor. Higher CO emissions also suggest that there may be higher unburned hydrocarbon (UHC) emission and hence lower combustion efficiency for the forward flow configuration 'FP2'. In the novel non-premixed mode, higher NO emissions were observed for both forward and reverse flow configurations (see Fig. 13a) with highest emissions observed for the reverse flow configuration 'RO'. Forward flow configuration 'FO' resulted in lower CO levels (about 200 ppm) as compared to the forward flow configuration 'FS2' but higher CO emissions as compared to the reverse flow configuration 'RO' (see Fig. 13b). This may be due to higher residence time for the opposed flow configuration ('FO') as compared to the configuration where both air and fuel are injected from same side ('FS2'). This was also confirmed from the numerical simulations where configuration 'FO' had higher residence time as compared to configuration 'FS2' [26]. Reverse flow configuration 'RO' had lower CO emissions as compared to the forward flow

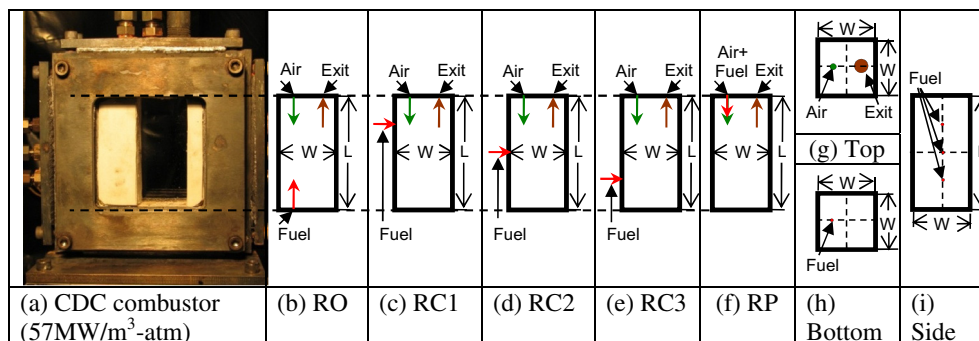


Fig. 14. High thermal intensity CDC combustor (57 MW/m<sup>3</sup> atm, 6.25 kW) (a) photograph and (b–i) schematic diagrams of different geometries examined.

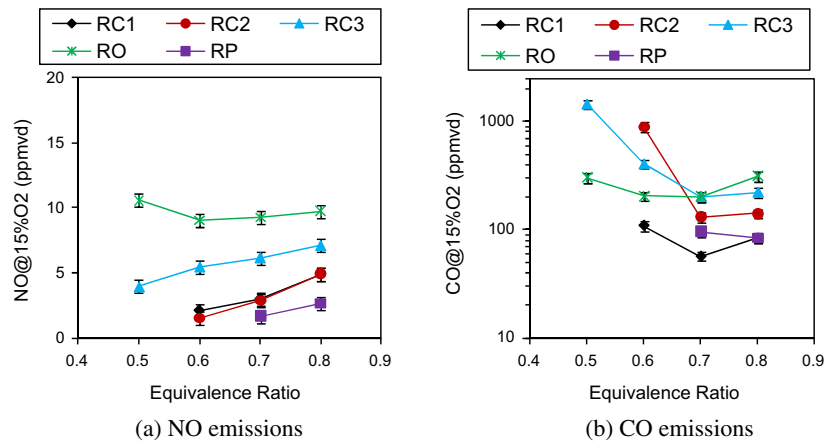


Fig. 15. (a) NO emissions and (b) CO emissions for CDC combustor at thermal intensity of  $57 \text{ MW/m}^3 \text{ atm}$  and heat load of  $6.25 \text{ kW}$ .

configuration 'FO' and this suggests favorable residence time for reverse flow configuration as compared to forward flow configuration. The reverse flow configuration was further explored at higher thermal intensities and enhanced mixing conditions to achieve lower NO and CO emissions and is discussed next. It can also be observed that NO emissions increase with decrease in equivalence ratio for the configuration 'RO' and this suggests that further investigations are required to achieve uniformly distributed reactions as for a perfectly stirred reactor NO emission is expected to increase with increase in equivalence ratio.

### 5.3. Combustor operation at $57 \text{ MW/m}^3 \text{ atm}$

Different reverse flow configurations were investigated at thermal intensity of  $57 \text{ MW/m}^3 \text{ atm}$ . The details are shown in Fig. 14. It can be noted that configurations where fuel is injected in cross-flow with respect to air injection are also included ('RC1', 'RC2' and 'RC3') in addition to configuration 'RO' and 'RP'. The heat load here is fixed at  $6.25 \text{ kW}$ . Fuel injection velocity is  $97 \text{ m/s}$  and air injection velocity varied from  $128$  to  $205 \text{ m/s}$  to cause a subsequent variation in the equivalence ratio of  $0.8$ – $0.5$  respectively. Further details of experimental conditions are given elsewhere [27].

Fig. 15 shows NO and CO emission at thermal intensity of  $57 \text{ MW/m}^3 \text{ atm}$ . From the figure it can be observed that the novel

premixed mode 'RP' resulted in ultra-low NO (about  $1 \text{ ppm}$ ) and low CO (about  $100 \text{ ppm}$ ) emission levels. It may be noted that the reverse flow configuration in premixed mode operating at thermal intensity of  $28 \text{ MW/m}^3 \text{ atm}$  also resulted in NO emission of  $1 \text{ ppm}$  but lower CO emission (about  $50 \text{ ppm}$ ) (see Fig. 13b) and this further suggests that increase in thermal intensity results in lower residence time to result in higher CO emissions.

From Fig. 15a it can be observed that the novel non-premixed configuration 'RO' results in high NO emissions (more than  $10 \text{ ppm}$ ). NO emission level decreases with increase in equivalence ratio and this is similar to the results obtained for reverse flow configuration 'RO' investigated at thermal intensity of  $28 \text{ MW/m}^3 \text{ atm}$  (see Fig. 13a). This suggests that further investigations are required to achieve reactions closer to distributed regime as for the perfectly stirred reactor case NO emission level is expected to increase with increase in equivalence ratio.

In the cross flow mode ('RC1', 'RC2', 'RC3') as the fuel injection location is shifted closer to the air injection port; higher cross-flow velocity will be encountered resulting in better fuel/oxidizer mixing. This is expected to result in lower NO and CO emissions. This was also observed experimentally as seen from Fig. 15a. Configuration 'RC1' resulted in ultra-low NO (about  $3 \text{ ppm}$ ) and low CO (about  $60 \text{ ppm}$ ) emissions. This suggests that reverse flow configuration in cross-flow provides lower NO and CO emissions even at high thermal intensity in the non-premixed mode. It

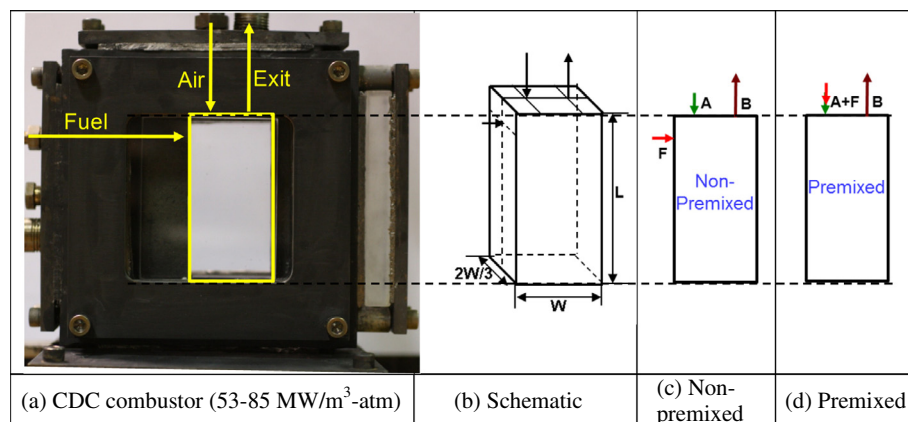


Fig. 16. High thermal intensity CDC combustor (range is  $53$ – $85 \text{ MW/m}^3 \text{ atm}$ ) (a) photograph, (b) schematic, (c) non-premixed and (d) premixed mode, heat load range is  $3.91$ – $6.25 \text{ kW}$ .



may be noted that for configuration 'RC1', NO emission level increases with increase in equivalence ratio and that emission levels are closer to the novel premixed flow mode so that this configuration is more representative of more distributed reactions for this configuration (see Fig. 15a). The reverse cross flow 'RC' configuration was further investigated at higher thermal intensities and is discussed next.

## 6. High thermal intensity combustor (53–453 MW/m<sup>3</sup> atm)

### 6.1. Combustor operation at 53–85 MW/m<sup>3</sup> atm

From the previous investigations on the forward flow as well as reverse flow configurations it was found that the reverse flow geometry results in higher residence time which helped to achieve lower CO levels as compared to the forward flow configurations. Fuel injection in cross flow results in faster mixing of fuel with the oxidant stream to results in lower NO and CO emission levels.

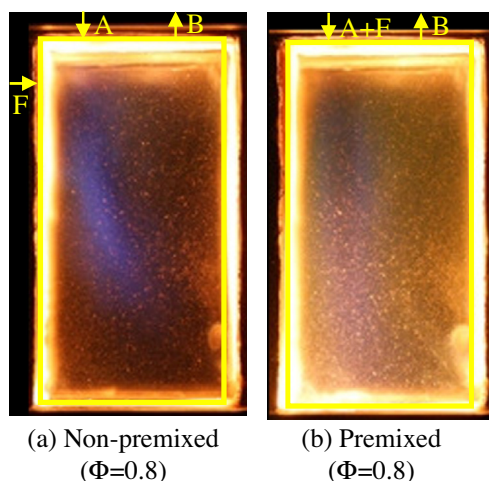


Fig. 17. Global images for CDC combustor (at 85 MW/m<sup>3</sup> atm, 6.25 kW) for (a) non-premixed and (b) premixed modes.

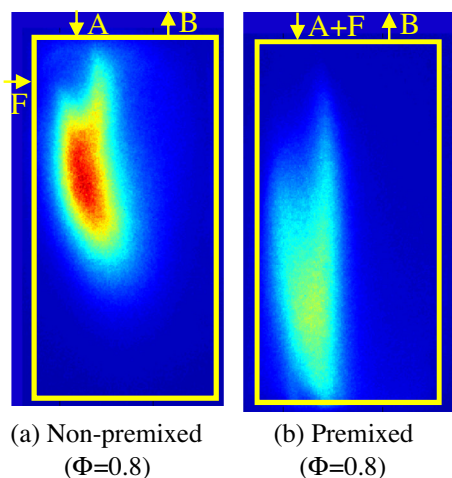


Fig. 18. OH\* images for CDC combustor (85 MW/m<sup>3</sup> atm, 6.25 kW) for (a) non-premixed and (b) premixed modes.

This suggests that reverse cross-flow configuration could be further investigated to achieve enhanced performance of the CDC combustor with near zero pollutants emission. The selected geometry operating under reverse cross-flow configuration is shown in Fig. 16. The depth of the combustor for reverse cross-flow geometry was reduced (see Fig. 16b) from the previously examined geometry (see Fig. 14g and h) to result in higher thermal intensity range of 53–85 MW/m<sup>3</sup> atm. The fuel injection location was shifted closer to the air injection location in order to enhance the mixing and achieve even better combustion characteristics (see Fig. 16b) as compared to fuel injection location for the flow configuration 'RC1' (see Fig. 14i). The air injection diameter was increased as compared to the one used in previous investigation to help reduce the pressure drop across the combustor.

The air inlet temperature was increased from 300 K to 600 K to simulate air preheats due to near isentropic compression in the gas turbine compressor. The air flow rate was kept constant; however, the fuel flow rate was changed to simulate different power setting of the gas turbine combustor. It may be noted that in the previous investigations reported in this paper the heat load (thermal intensity) was kept constant; however, in the present investigation the heat load as well as thermal intensity was changed with the change in equivalence ratio. This resulted in combustor operation at heat load variation from 6.25 to 3.91 kW for equivalence ratio variation from 0.8 to 0.5. The thermal intensity was varied from 85 to 53 MW/m<sup>3</sup> atm. Air injection velocity was 92 m/s at 600 K and fuel injection velocity was varied from 97 to 61 m/s for equivalence ratio variation of 0.8–0.5. The details of the experimental conditions can be found elsewhere [31].

Global reaction zone photographs at equivalence ratio of 0.8 for both non-premixed and premixed modes of colorless distributed combustion (CDC) are shown in Fig. 17. In the novel non-premixed mode bluish region near the location of fuel injection could be observed suggesting the presence of reaction zone. Almost colorless reaction zone is observed for the novel premixed flow mode where higher glow from combustor walls could be observed.

Fig. 18 shows the location of reaction zone (OH\* chemiluminescence) in the non-premixed and premixed flow modes for the CDC combustor at equivalence ratio of 0.8. From the figure it can be observed that the reaction zone is stabilized where fuel mixes with the air jet in cross-flow along with the hot gases. For the non-premixed mode the OH\* intensity is much higher as compared to the premixed flow mode suggesting that the reaction zone is operating at higher equivalence ratio in the non-premixed mode as compared to the overall equivalence ratio (as in premixed mode case) and that further improvements in mixing are possible for our quest to achieve even lower NO and CO emissions in the non-premixed mode. It may also be noted that the reaction zone is present in a limited region of the combustor and this suggests that further increase in thermal intensity is possible so that the reaction zone occupies almost complete combustor. This is an area of active examination by our group.

The emissions for the both non-premixed and premixed flow modes at air preheat temperature of 600 K are shown in Fig. 19. Higher air preheat temperature (600 K vs 300 K) resulted in extension of lean operational limit of the combustor so that the combustor could be operated at equivalence ratio of 0.5 in both the premixed and non-premixed modes. At this operating condition the NO emission was about 4 ppm in the non-premixed mode, about 1 ppm in the premixed mode and CO emission were about 30 ppm in both the non-premixed and premixed flow modes. The pressure drop across the combustor was less than 5% with pressure fluctuations of less than 0.025% [31]. These results suggest that the combustor could be operated at thermal intensity of 53 MW/m<sup>3</sup> atm to provide very low NO and CO emission in addition to



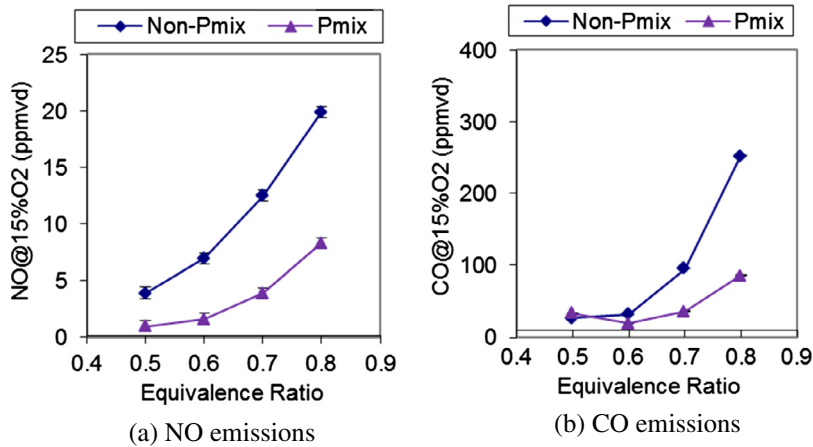


Fig. 19. (a) NO and (b) CO emissions in non-premixed and premixed conditions for the CDC combustor ( $53\text{--}85\text{ MW/m}^3\text{ atm}$ ,  $3.91\text{--}6.25\text{ kW}$ ).

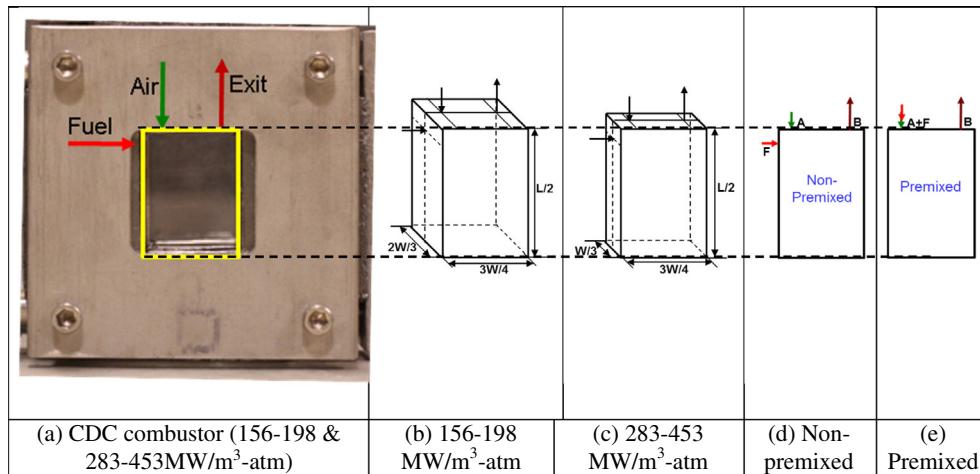


Fig. 20. (a) High thermal intensity CDC combustor and schematic for, (b)  $156\text{--}198\text{ MW/m}^3\text{ atm}$ ,  $4.3\text{--}5.47\text{ kW}$ , (c)  $283\text{--}453\text{ MW/m}^3\text{ atm}$ ,  $3.9\text{--}6.25\text{ kW}$ , (d) non-premixed and (e) premixed mode.

low pressure drop across the combustor with low pressure fluctuations.

## 6.2. Combustor operation at $156\text{--}198\text{ MW/m}^3\text{ atm}$ and $283\text{--}453\text{ MW/m}^3\text{ atm}$

Further increase in thermal intensity was achieved by reducing the length as well as the width of the combustor (see Fig. 20b and c) as compared to previous case (see Fig. 16b) for the reverse cross-flow geometry. It may be noted that the width of the combustor was reduced to help alleviate zones on the left side of air jet as well as from the right side of the combustor. The region on left side of the air jet was observed to recirculate gases which could be detrimental to combustor performance [31]. The combustor operating at thermal intensity range of  $283\text{--}453\text{ MW/m}^3\text{ atm}$  (Fig. 16c) had half the depth of combustor operating at thermal intensity range of  $156\text{--}198\text{ MW/m}^3\text{ atm}$  (Fig. 16b). The combustor operating at thermal intensity range of  $156\text{--}198\text{ MW/m}^3\text{ atm}$  had equivalence ratio variation of

$0.55\text{--}0.7$  and heat load range of  $4.3\text{--}5.47\text{ kW}$ . The combustor operating at thermal intensity range of  $283\text{--}453\text{ MW/m}^3\text{ atm}$  had equivalence ratio variation of  $0.5\text{--}0.8$  and heat load range of  $3.9\text{--}6.25\text{ kW}$ . For both the combustors the fuel injection location was shifted further towards the air injection location (see Fig. 20b) to enhance mixing as compared to the geometry examined earlier (see Fig. 16b). Air injection velocity was  $92\text{ m/s}$  and the air injection temperature was  $600\text{ K}$ . The fuel injection diameter for the higher thermal intensity combustor was increased to reduce the jet velocity and hence reduce the distortion of the air jet in cross flow [33]. Further details of experimental conditions can be found elsewhere [32,33].

The emission levels of NO and CO for both the high intensity combustors are presented in Fig. 21. It can be observed that at equivalence ratio of  $0.6$ , corresponding to thermal intensity of  $170\text{ MW/m}^3\text{ atm}$ , the combustor produced  $8\text{ ppm}$  NO in non-premixed mode and  $3\text{ ppm}$  in premixed mode, and about  $100\text{ ppm}$  CO in both the modes. For higher thermal intensity combustor operating at  $340\text{ MW/m}^3\text{ atm}$  at equivalence ratio of  $0.6$ , the

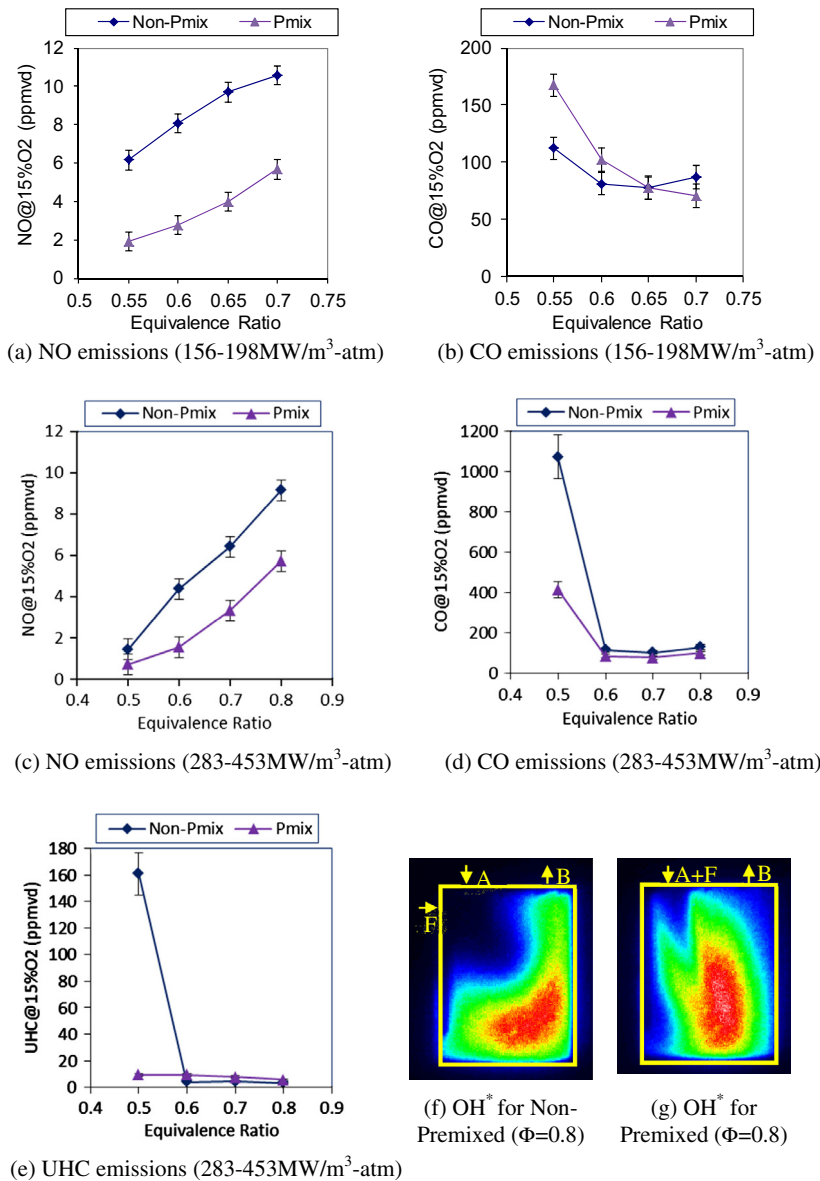


**Fig. 21.** NO and CO emissions in non-premixed and premixed conditions for thermal intensity range from (a and b) 156–198 MW/m<sup>3</sup> atm, 4.3–5.47 kW, (c and d) 283–453 MW/m<sup>3</sup> atm, 3.9–6.25 kW, (e) UHC emissions and (f and g) OH\* distribution.

combustor produced 4 ppm NO in non-premixed mode and 2 ppm in premixed mode, and about 100 ppm CO in both the modes. It may be noted that at thermal intensity of 144 MW/m<sup>3</sup> atm the NO emission level was 52 ppm and CO emission level was 520 ppm for the trapped vortex combustor [22]. Unburned hydrocarbons (UHC) were also measured for combustor operating at thermal intensity range of 283–453 MW/m<sup>3</sup> atm. The results showed less than 10 ppm UHC emission level at equivalence ratio of 0.6 and thermal intensity of 340 MW/m<sup>3</sup> atm, see Fig. 21e. OH\* distribution for both non-premixed and premixed cases is shown in Fig. 21f and g. It can be observed that for both the cases reaction zone occupies almost the complete volume of the combustor suggesting very high thermal intensity. Continued development on the distributed combustion will help achieve our goal of near zero emissions of all the pollutants from the fuel to energy thermal conversion in gas turbine applications.

## 7. Role of thermal intensity variation of 5–340 MW/m<sup>3</sup> atm

The effect of thermal intensity variation on the operation of CDC combustors which were discussed in previous sections is discussed by comparing different reverse flow geometries operating at thermal intensities in the range of 5–340 MW/m<sup>3</sup> atm. These combustors are compared in premixed mode of operation to avoid the effect of fuel/air mixing on combustion characteristics and hence only the effect of thermal intensity can be examined. Inlet temperature of air and fuel mixture was same and equal to 300 K for all the cases. The combustor at 340 MW/m<sup>3</sup> atm at air and fuel mixture inlet temperature of 300 K was not able to sustain stable combustion at these conditions and hence the corresponding results are not included here. The geometries which were able to support stable combustion are shown in Fig. 22. The corresponding heat load and inlet velocity are also included. Note that the thermal

$T_{\text{air+fuel}}$	300K	300K	300K	300K	300K	300K
$V_{\text{air+fuel}}$	157m/s	157m/s	157m/s	49m/s	157m/s	49m/s
$D_{\text{air+fuel}}$	3/16inch	3/16inch	3/16inch	5/16inch	3/16inch	5/16inch
Heat load @ $\Phi=0.7$	25kW	6.25kW	6.25kW	5.47kW	6.25kW	5.47kW
Heat load @ $\Phi=0.8$	25kW	6.25kW	6.25kW	6.25kW	6.25kW	6.25kW
Thermal intensity @ $\Phi=0.7$	(a)5MW/m <sup>3</sup> -atm	(b)28MW/m <sup>3</sup> -atm	(c)57MW/m <sup>3</sup> -atm	(d)74MW/m <sup>3</sup> -atm	(e)85MW/m <sup>3</sup> -atm	(f)198MW/m <sup>3</sup> -atm
Thermal intensity @ $\Phi=0.8$	(a)5MW/m <sup>3</sup> -atm	(b)28MW/m <sup>3</sup> -atm	(c)57MW/m <sup>3</sup> -atm	(d)85MW/m <sup>3</sup> -atm	(e)85MW/m <sup>3</sup> -atm	(f)227MW/m <sup>3</sup> -atm

Fig. 22. Reverse flow configurations investigated for premixed mode at thermal intensity range from 5 to 198 MW/m<sup>3</sup> atm at equivalence ratio of 0.7.

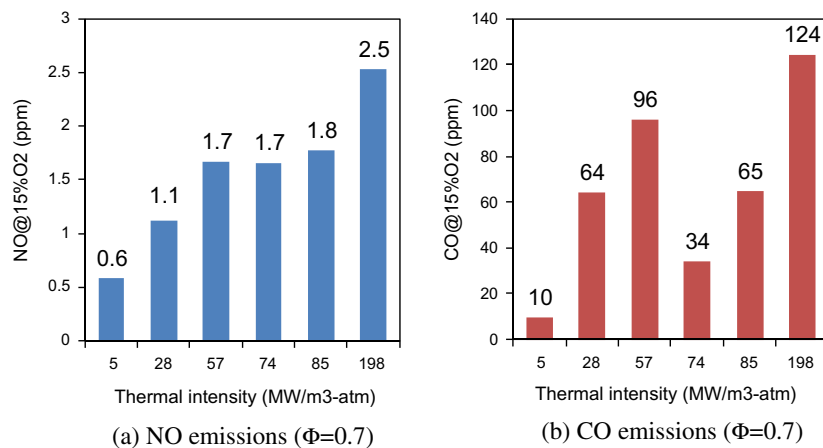


Fig. 23. (a) NO and (b) CO emissions for premixed flow mode corresponding to thermal intensity range of 5–198 MW/m<sup>3</sup> atm.

intensity is provided for equivalence ratio of 0.7 and 0.8. For combustors shown in Fig. 22d and f thermal intensity is different at equivalence ratio of 0.7 and 0.8, and this is because for these cases the fuel flow rate was varied while keeping the air flow rate same. However, for other combustors air flow rate was varied while fuel flow rate was kept same to achieve different equivalence ratios, and hence for these cases thermal intensity is same at the two equivalence ratios.

Emission levels were measured at equivalence ratio of 0.7. Fig. 23 shows NO and CO emissions at equivalence ratio of 0.7 for the range of thermal intensity investigated. From the figure it can be seen that the NO emissions are very low (less than 3 ppm) for all the cases; however, there is a significant variation

in CO emissions. NO emission increases with increase in thermal intensity and this may be due to relatively lower heat losses at higher thermal intensity resulting in higher gas temperatures and subsequently higher NO emissions. At thermal intensity of 5 MW/m<sup>3</sup> atm CO emission is only 10 ppm and it increases to 64 ppm at thermal intensity of 28 MW/m<sup>3</sup> atm and to 96 ppm at thermal intensity of 57 MW/m<sup>3</sup> atm. It may be noted that the air injection temperature, injection velocity as well as the injection diameter is same for these three cases. This increase in CO is possibly due to lower residence time at higher thermal intensities (refer Fig. 5a).

The average residence time for different combustors is shown in Fig. 24a and from the figure it can be noted that the residence time

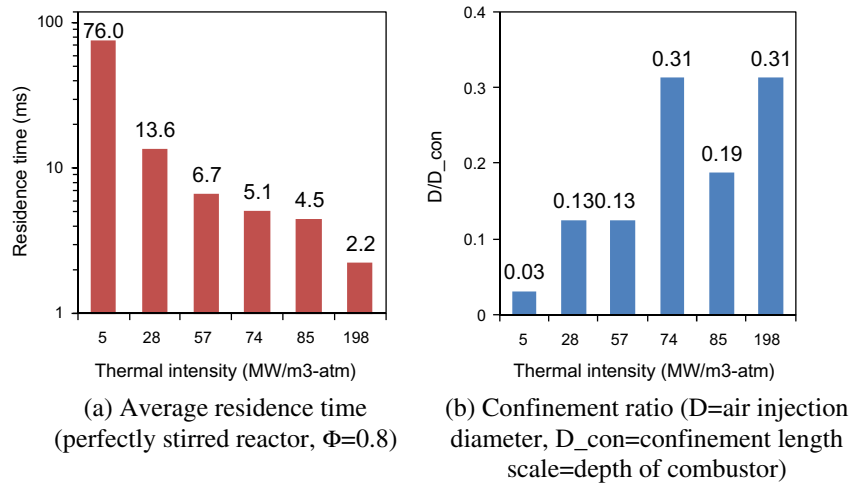


**Fig. 24.** (a) Average residence time and (b) confinement ratio for different combustors at thermal intensity range from 5 to 227 MW/m³ atm.

decreases from 76 to 6.7 ms with increase in thermal intensity from 5 to 57 MW/m³ atm. Residence time characteristics were obtained numerically at equivalence ratio of 0.8. Residence time distribution is shown in Fig. 25a and b. From residence time distribution plots also it can be noted that the combustor with higher thermal intensity has higher fraction of gases having lower residence time, which will further result in higher CO emissions (see Fig. 5b).

However, an interesting trend can be observed with respect to CO emission as the thermal intensity is increased from 57 MW/m³ atm (see Fig. 22c) to 85 MW/m³ atm (see Fig. 22e). In this case

even though the residence time decreases from 6.7 ms to 4.5 ms the CO emission decreases from 96 ppm to 65 ppm. At higher thermal intensity the effect of confinement is expected to play an important role on the flow field inside the combustor. The confinement ratio (ratio of air injection diameter and confinement depth) for different combustors is presented in Fig. 24b. It can be observed that as the thermal intensity is increased from 57 MW/m³ atm to 85 MW/m³ atm the confinement ratio increases from 0.13 to 0.19. At thermal intensity of 5 MW/m³ atm the confinement ratio was only 0.03 and the jets is expected to behave closer to a free jet. From Fig. 5c we can observe that at confinement ratio of about

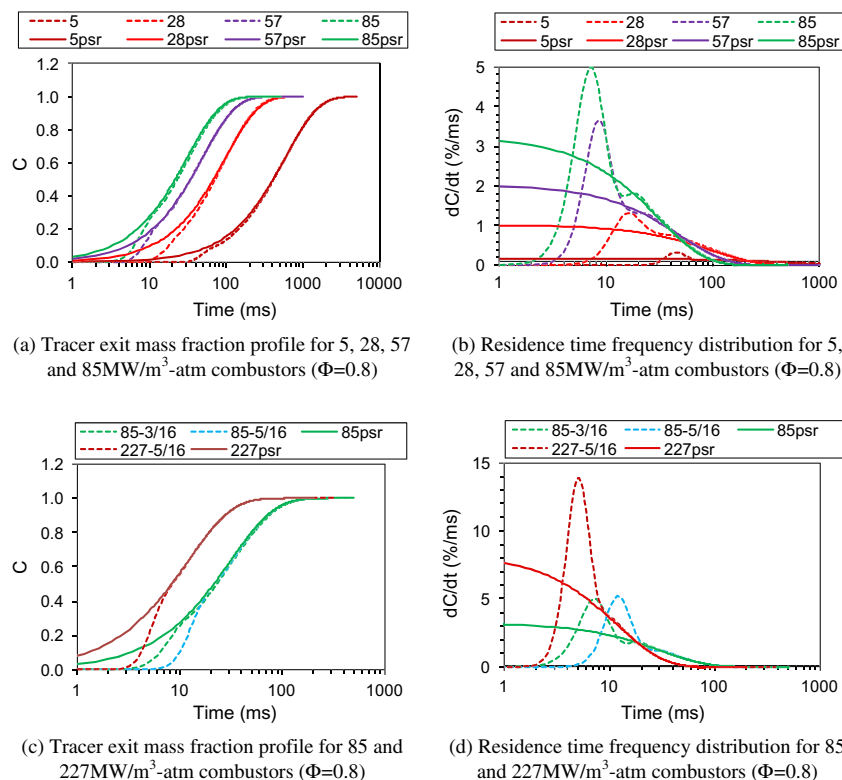


**Fig. 25.** Residence time characteristics for the reverse flow combustors investigated, psr = perfectly stirred reactor.

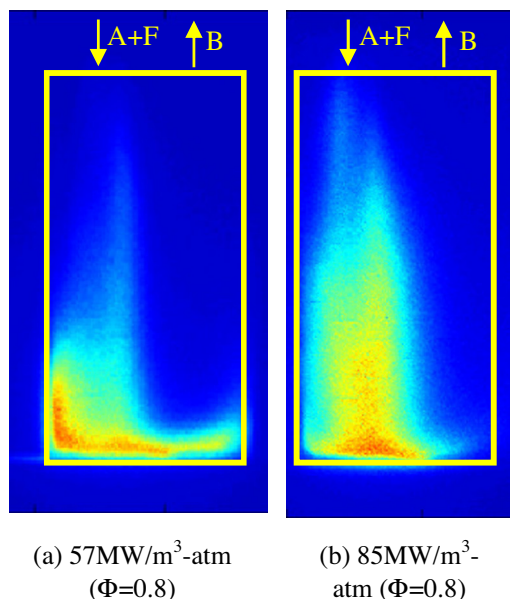


**Fig. 26.** OH\* distribution at thermal intensity of (a) 57 MW/m<sup>3</sup> atm, 6.27 kW and (b) 85 MW/m<sup>3</sup> atm, 6.25 kW.

0.1 the jet decay is very similar to the free jet decay, however, as the confinement ratio is increased to 0.2 and 0.3 the jet decay is much more rapid. This suggests that as the confinement ratio is increased the jet decay is very fast and this may result in anchoring of reaction zone closer to the air injection location. Location of reaction zone can be obtained from the OH\* chemiluminescence imaging technique and the results are reported in Fig. 26. OH\* distribution were obtained at equivalence ratio of 0.8. A shift of reaction zone towards the air injection location for thermal intensity of 85 MW/m<sup>3</sup> atm (see Fig. 26b) as compared to the thermal intensity of 57 MW/m<sup>3</sup> atm (see Fig. 26a) can be observed. This shift in reaction zone may result in longer residence time available for the hot gases before escaping from the combustor to subsequently result in lower CO emissions. Hence with careful design of the combustor lower CO emissions could be achieved even at higher thermal intensities.

With increase in air injection diameter (see Fig. 22d and f) the confinement ratio is further increased to 0.3 and this result in lower CO emission (34 ppm at thermal intensity of 74 MW/m<sup>3</sup> atm). Hence an increase in the air injection diameter can provide beneficial role to not only reduce the pressure drop across the combustor but also to move reaction zone closer to the air injection location and increase the residence time of gases inside the combustor. This can be also be observed from the residence time profiles shown in Fig. 25c and d. For the cases with same thermal intensity (85 MW/m<sup>3</sup> atm at equivalence ratio of 0.8) but different air injection diameter (3/16 in. vs 5/16 in.) the combustor having larger air injection diameter has lower fraction of gases having lower residence time. Note that the case 85-5/16 corresponds to thermal intensity of 74 MW/m<sup>3</sup> atm at equivalence ratio of 0.7 (see Fig. 22d).

Comparing the case of combustor operating at thermal intensity of 74 MW/m<sup>3</sup> atm and 198 MW/m<sup>3</sup> atm (see Fig. 22d and f respectively) one can observe that CO emission increases from 34 ppm to 124 ppm, respectively. It can be noted that for these two cases the

confinement ratio is the same (about 0.31) and hence increase in thermal intensity resulted in smaller residence time (2.2 ms as compared to 4.5 ms) that will result in higher CO emissions, as observed here. It may be noted that increase in thermal intensity also reduces the gas recirculation significantly and this may affect the stability characteristics and operational range of the CDC combustor (see Fig. 5c). As mentioned earlier, the combustor at 340 MW/m<sup>3</sup> atm, with air inlet temperature of 300 K, was not able to sustain stable combustion and this suggest that increase in thermal intensity can be realized only up to certain thermal intensities. A thermal intensity of 340 MW/m<sup>3</sup> atm is about an order of magnitude higher than that used in current gas turbine engines.

## 8. Conclusions

Role of thermal intensity variation from 5 to 453 MW/m<sup>3</sup> atm has been investigated under both premixed and non-premixed flow modes with the focus to further develop distributed combustion conditions. Development of high thermal intensity distributed combustion with no visible signatures (colorless distributed combustion (CDC)) or green combustion turbine (having green color flame) for gas turbine applications requires careful design consideration on the role of various input and operational parameters for ultra-low NO<sub>x</sub> and CO emissions. Different flow configurations such as forward and reverse flow have been discussed in this investigation. It was observed that the operation of combustor at higher thermal intensity results in lower residence time and lower gas recirculation to pose the problem of flame stabilization and sustained combustion and results in higher CO emissions. The reverse flow configuration results in favorable residence time distribution which helps to reduce CO emission levels. Favorable location of the reaction zone and advantageous residence time distribution was observed to result in ultra-low CO emissions even at high thermal intensities. In non-premixed mode the fuel injection in cross-flow resulted in faster mixing between the fuel and oxidizer to result in lower NO and CO emissions. A systematic examination of the flow configurations resulted in desirable combustion characteristics even at very high thermal intensities of up to 453 MW/m<sup>3</sup> atm for improved performance and low emissions. The high thermal intensity combustor operating at thermal intensity of 340 MW/m<sup>3</sup> atm in reverse cross-flow configuration resulted in very low NO (about 4 ppm in non-premixed and 2 ppm in premixed) and CO emissions (about 100 ppm in both modes). At such high thermal intensity the reaction zone was observed to be present in entire combustor. Our continued efforts have shown near zero emissions at high combustion intensities that are commensurable with currently used combustion intensities in gas turbine combustors.

## Acknowledgments

This research was supported by ONR, Program Managers, Dr. Gabriel D. Roy and Dr. Clifford Bedford, and by Army under MPCA. Their support is gratefully acknowledged. The authors also acknowledge the support provided by Reaction Design for the Chemkin-PRO code.

## Appendix A. Operational characteristics of low emission combustor

See Tables 1 and 2.



**Table 1**

Combustor designs reported in literature.

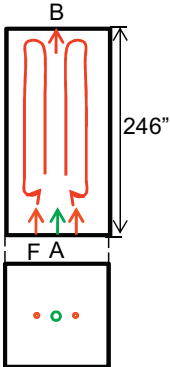
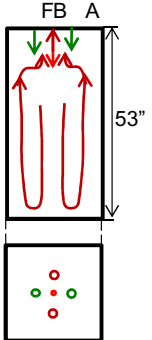
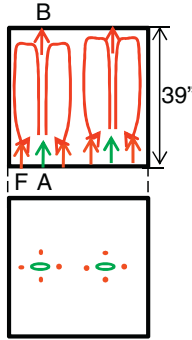
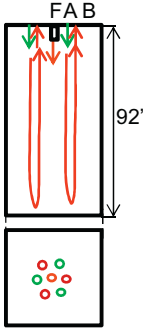
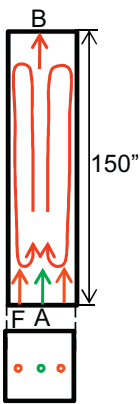
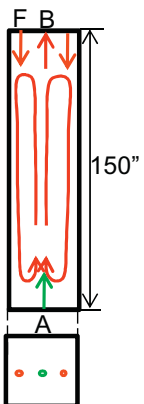
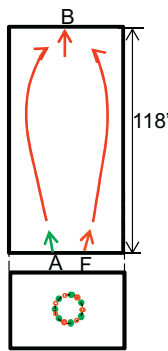
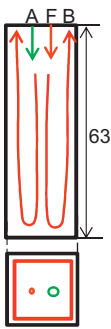
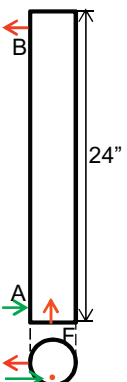
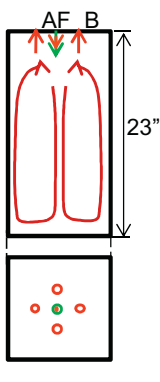
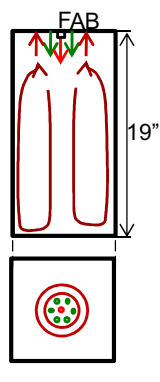
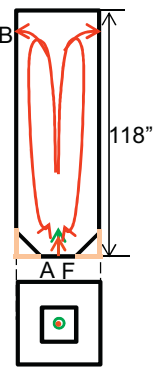
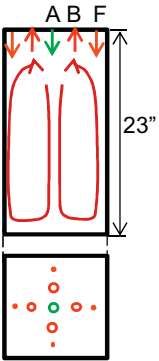
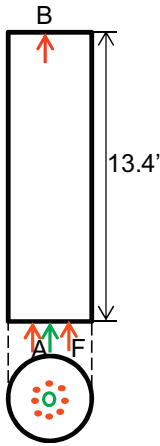
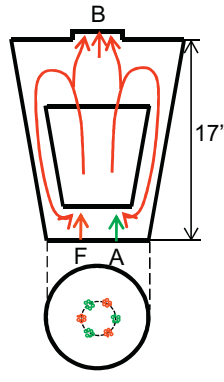
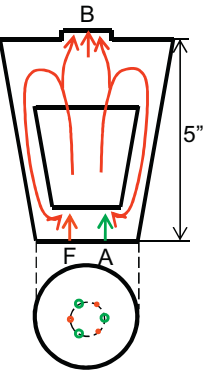
	 <p>(1) MILD, Weber et al., IFRF, 2005</p>	 <p>(2) FLOX, Colorado et al., U Antioquia, 2010</p>	 <p>(3) HiTAC, Gupta et al., NFK, 2003</p>	 <p>(4) FLOX, Wunning et al., WS GmbH, 1997</p>
Configuration	FS	RS	FS	RS
Thermal intensity	0.02 MW/m <sup>3</sup> -atm	0.05 MW/m <sup>3</sup> -atm	0.06 MW/m <sup>3</sup> -atm	0.07 MW/m <sup>3</sup> -atm
Heat load	580 kW	20 kW	58 kW	200 kW
Fuel	Natural gas	Natural gas	Natural gas	Natural gas
Pressure	1 atm	1 atm	1 atm	1 atm
Air velocity	85 m/s	79 m/s	74 m/s	–
Fuel velocity	100 m/s	81 m/s	40 m/s	–
Air diameter	124 mm	24.4 mm	29.1 mm	–
Fuel diameter	11.3 mm	3.2 mm	2.7 mm	–
$\tau_{air}$ (D/U)	1.46 ms	0.309 ms	0.393 ms	–
$\tau_{fuel}$ (D/U)	0.113 ms	0.040	0.068 ms	–
Air temperature	1100 K	1600 K	810 K	1400 K
Fuel temperature	300 K	300 K	300 K	300 K
NO <sub>x</sub> @15%O <sub>2</sub>	9 ppm ( $\Phi = 1$ )	1 ppm ( $\Phi = 0.8$ )	44 ppm ( $\Phi = 0.8$ )	11 ppm ( $\Phi = 0.9$ )
CO@15%O <sub>2</sub>	<10 ppm ( $\Phi = 1$ )	<10 ppm ( $\Phi = 0.8$ )	–	–
	 <p>(5) HiTAC, Gupta et al., NFK, 2003</p>	 <p>(6) HiTAC, Gupta et al., NFK, 2003</p>	 <p>(7) FODI, Sobiesiak et al., Queen's, 1998</p>	 <p>(8) FODI, He et al., Queen's, 2008</p>
Configuration	FS	FO	FS	RS
Thermal intensity	0.1 MW/m <sup>3</sup> -atm	0.1 MW/m <sup>3</sup> -atm	0.1 MW/m <sup>3</sup> -atm	0.1 MW/m <sup>3</sup> -atm
Heat load	350 kW	350 kW	368 kW	32 kW
Fuel	Natural gas	Natural gas	Natural gas	Natural gas
Pressure	1 atm	1 atm	1 atm	1 atm
Air velocity	–	–	145 m/s	118 m/s
Fuel velocity	–	–	51 m/s	41 m/s
Air diameter	–	–	19.1 mm	12.7 mm
Fuel diameter	–	–	6.35 mm	5.4 mm
$\tau_{air}$ (D/U)	–	–	0.131 ms	0.107 ms
$\tau_{fuel}$ (D/U)	–	–	0.125 ms	0.132 ms
Air temperature	324 K	1400 K	1400 K	650 K
Fuel temperature	288 K	300 K	300 K	300 K
NO <sub>x</sub> @15%O <sub>2</sub>	9 ppm ( $\Phi = 0.8$ )	8 ppm ( $\Phi = 0.8$ )	12 ppm ( $\Phi = 0.8$ )	3 ppm ( $\Phi = 0.6$ )
CO@15%O <sub>2</sub>	<10 ppm ( $\Phi = 0.8$ )	10 ppm ( $\Phi = 0.8$ )	–	34 ppm ( $\Phi = 0.6$ )

Table 1 (continued)

				
	(9) PAWC, Yetter et al., Princeton, 2000	(10) MILD, Mi et al., U. Ad. 2009	(11) MILD, Dally et al., U. Ad., 2004	(12) FLOX, Xing et al., UST China, 2007
Configuration	SWIRL	RS	RS	FS (coaxial)
Thermal intensity	0.1 MW/m <sup>3</sup> -atm	0.2 MW/m <sup>3</sup> -atm	0.2 MW/m <sup>3</sup> -atm	0.3 MW/m <sup>3</sup> -atm
Heat load	0.54 kW	10 kW	7 kW	1000 kW
Fuel	Methane	Natural gas	Methane	Natural gas
Pressure	1 atm	1 atm	1 atm	1 atm
Air velocity	17 m/s	21 m/s	85 m/s	–
Fuel velocity	1 m/s	10 m/s	15 m/s	63 m/s
Air diameter	11.2 mm	4.4 mm	5 mm	–
Fuel diameter	4.8 mm	7.2 mm	4 mm	–
$\tau_{air}$ (D/U)	0.658 ms	0.210 ms	0.059 ms	–
$\tau_{fuel}$ (D/U)	4.8 ms	0.720 ms	0.267 ms	–
Air temperature	300 K	300 K	723 K	1352 K
Fuel temperature	300 K	300 K	293 K	300 K
NO <sub>x</sub> @15%O <sub>2</sub>	5 ppm ( $\Phi = 0.1$ )	1 ppm ( $\Phi = 0.8$ )	7 ppm ( $\Phi = 0.8$ )	26 ppm ( $\Phi = 0.9$ )
CO@15%O <sub>2</sub>	225 ppm ( $\Phi = 0.1$ )	<10 ppm ( $\Phi = 0.8$ )	–	<10 ppm ( $\Phi = 0.9$ )
				
	(13) MILD, Szego et al., U. Ad., 2009	(14) FLOX, Verissimo et al., TU Lisbon, 2011	(15) HILE, Kumar et al., IISc, 2005	(16) HILE, Kumar et al., IISc, 2002
Configuration	RS	FLOX	FS	FS
Thermal intensity	0.3 MW/m <sup>3</sup> -atm	3.8 MW/m <sup>3</sup> -atm	5.6 MW/m <sup>3</sup> -atm	10 MW/m <sup>3</sup> -atm
Heat load	15 kW	10 kW	150 kW	3 kW
Fuel	Natural gas	Methane	LPG	LPG
Pressure	1 atm	1 atm	1 atm	1 atm
Air velocity	20 m/s	96 m/s	95 m/s	79 m/s
Fuel velocity	40 m/s	6.2 m/s	243 m/s	60 m/s
Air diameter	26.6 mm	10 mm	5 mm	2 mm
Fuel diameter	2 mm	2 mm	0.7 mm	0.5 mm
$\tau_{air}$ (D/U)	1.33 ms	0.104 ms	0.052 ms	0.025 ms
$\tau_{fuel}$ (D/U)	0.05 ms	0.323 ms	0.003 ms	0.008 ms
Air temperature	300 K	723 K	973 K	300 K
Fuel temperature	300 K	293 K	300 K	300 K
NO <sub>x</sub> @15%O <sub>2</sub>	14 ppm ( $\Phi = 0.8$ )	4 ppm ( $\Phi = 0.9$ )	7.5 ppm ( $\Phi = 1$ )	4 ppm ( $\Phi = 0.9$ )
CO@15%O <sub>2</sub>	<100 ppm ( $\Phi = 0.8$ )	12 ppm ( $\Phi = 0.9$ )	2900 ppm ( $\Phi = 1$ )	2200 ppm ( $\Phi = 0.9$ )

(continued on next page)

Table 1 (continued)

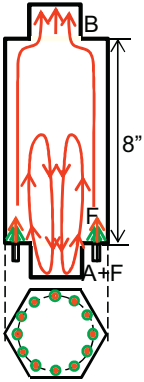
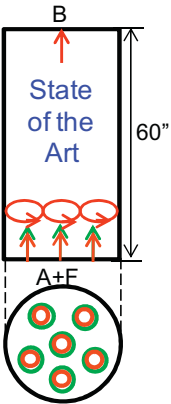
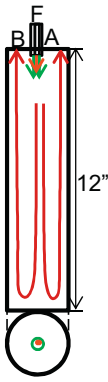
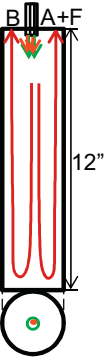
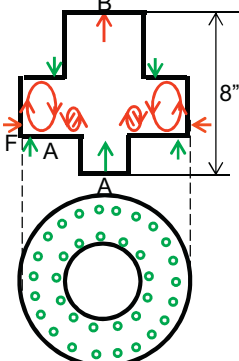
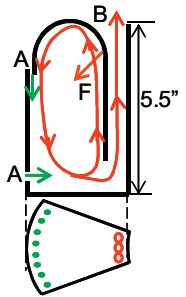
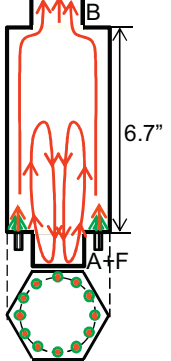
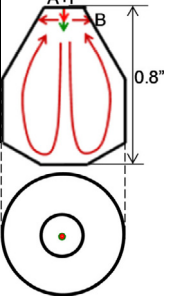
				
	(17) FLOX, Luckerath et al., DLR, 2008	(18) DLN-2.6, Vandervort, 2001	(19) SPRF, Bobba et al., GA-Tech, 2008	(20) SPRF, Bobba et al., GA-Tech, 2008
Configuration	FS (coaxial)	SWIRL (Premixed)	RS (coaxial)	RP
Thermal intensity	14 MW/m <sup>3</sup> -atm	15 MW/m <sup>3</sup> -atm	20 MW/m <sup>3</sup> -atm	20 MW/m <sup>3</sup> -atm
Heat load	475 kW	46,000 kW	20 kW	20 kW
Fuel	Natural gas	Natural gas	Natural gas	Natural gas
Pressure	20 atm	16 atm	1 atm	1 atm
Air velocity	160 m/s	70 m/s	110 m/s	120 m/s
Fuel velocity	78 m/s	–	30 m/s	–
Air diameter	4.5 mm	–	6.35 mm	6.35 mm
Fuel diameter	1 mm	–	4.7 mm	–
$\tau_{air}$ (D/U)	0.028 ms	–	0.058 ms	0.053 ms
$\tau_{fuel}$ (D/U)	0.013 ms	–	0.157 ms	–
Air temperature	450 K	735 K	631 K	450 K
Fuel temperature	–	300 K	–	450 K
NO <sub>x</sub> @15%O <sub>2</sub>	1 ppm ( $\Phi = 0.4$ )	<9 ppm ( $\Phi = 0.4$ )	1 ppm ( $\Phi = 0.5$ )	1 ppm ( $\Phi = 0.5$ )
CO@15%O <sub>2</sub>	<10 ppm ( $\Phi = 0.4$ )	<10 ppm ( $\Phi = 0.4$ )	<10 ppm ( $\Phi = 0.5$ )	<10 ppm ( $\Phi = 0.5$ )
				
	(21) RQL/TVC, Straub et al., NETL, 2005	(22) TVC, Melo et al., Technion, 2009	(23) FLOX, Lammel et al., DLR, 2010	(24) JSR, Shuman et al., UWashingon, 2000
Configuration	RO	RO	FP	RP
Thermal intensity	20 MW/m <sup>3</sup> -atm	25 MW/m <sup>3</sup> -atm	68 MW/m <sup>3</sup> -atm	90 MW/m <sup>3</sup> -atm
Heat load	700 kW	32 kW	750 kW	0.85 kW
Fuel	Natural gas	Methane	Natural gas	Natural gas
Pressure	10 atm	1 atm	7 atm	6.5 atm
Air velocity	–	75 m/s	90 m/s	80 m/s
Fuel velocity	–	83 m/s	–	–
Air diameter	–	4 mm	12 mm	1.4 mm
Fuel diameter	–	1 mm	–	–
$\tau_{air}$ (D/U)	–	0.053 ms	0.133 ms	0.018 ms
$\tau_{fuel}$ (D/U)	–	0.012 ms	–	–
Air temperature	573 K	644 K	300 K	673 K
Fuel temperature	–	300 K	300 K	–
NO <sub>x</sub> @15%O <sub>2</sub>	40 ppm ( $\Phi = 0.5$ )	6 ppm ( $\Phi = 0.5$ )	10 ppm ( $\Phi = 0.63$ )	3 ppm ( $\Phi = 0.6$ )
CO@15%O <sub>2</sub>	<10 ppm ( $\Phi = 0.5$ )	500 ppm ( $\Phi = 0.5$ )	<10 ppm ( $\Phi = 0.63$ )	50 ppm ( $\Phi = 0.6$ )

Table 1 (continued)

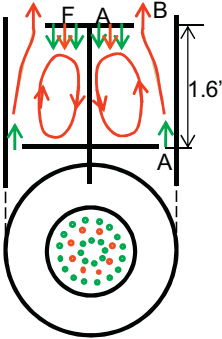
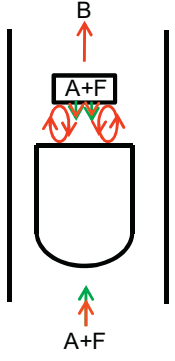
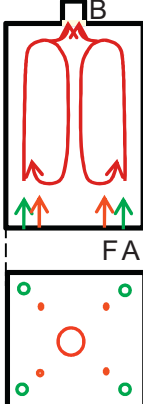
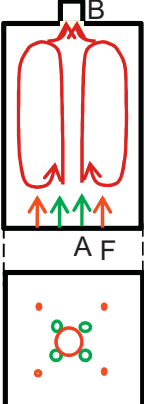
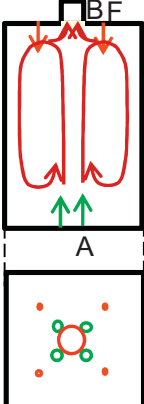
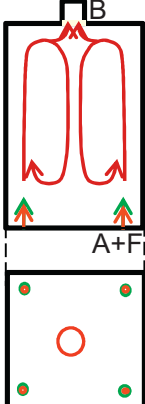
	 <p>(25) TVC, Hsu et al., AFRL, 1998</p>	 <p>(26) AVC, Edmonds et al., NETL, 2008</p>
Configuration	RS	RP
Thermal intensity	144 MW/m <sup>3</sup> -atm	–
Heat load	30 kW	1000 kW
Fuel	Propane	Natural gas
Pressure	1 atm	10 atm
Air velocity	48 m/s	81 m/s
Fuel velocity	17 m/s	–
Air diameter	2.29 mm	–
Fuel diameter	1.75 mm	–
$\tau_{air}$ (D/U)	0.048 ms	–
$\tau_{fuel}$ (D/U)	0.103 ms	–
Air temperature	300 K	603 K
Fuel temperature	300 K	–
NO <sub>x</sub> @15%O <sub>2</sub>	52 ppm ( $\Phi = 0.2$ )	4 ppm ( $\Phi = 0.55$ )
CO@15%O <sub>2</sub>	520 ppm ( $\Phi = 0.2$ )	<10 ppm ( $\Phi = 0.55$ )

Table 2

Combustor configurations investigated by Gupta, et al..

	 <p>(1) CDC, Gupta et al., UMD, 2010 FS</p>	 <p>(2) CDC, Gupta et al., UMD, 2010 FS</p>	 <p>(3) CDC, Gupta et al., UMD, 2010 FO</p>	 <p>(4) CDC, Gupta et al., UMD, 2010 FP</p>
Configuration	FS	FS	FO	FP
Thermal intensity	5 MW/m <sup>3</sup> -atm	5 MW/m <sup>3</sup> -atm	5 MW/m <sup>3</sup> -atm	5 MW/m <sup>3</sup> -atm
Heat load	25 kW	25 kW	25 kW	25 kW
Fuel	Methane	Methane	Methane	Methane
Pressure	1 atm	1 atm	1 atm	1 atm
Air velocity	128 m/s	128 m/s	128 m/s	139 m/s
Fuel velocity	97 m/s	97 m/s	97 m/s	–
Air diameter	4.8 mm	4.8 mm	4.8 mm	4.8 mm
Fuel diameter	1.6 mm	1.6 mm	1.6 mm	–
$\tau_{air}$ (D/U)	0.038 ms	0.038 ms	0.038 ms	0.035 ms
$\tau_{fuel}$ (D/U)	0.016 ms	0.016 ms	0.016 ms	–
Air temperature	300 K	300 K	300 K	300 K
Fuel temperature	300 K	300 K	300 K	–
NO <sub>x</sub> @15%O <sub>2</sub>	7 ppm ( $\Phi = 0.8$ )	3 ppm ( $\Phi = 0.8$ )	6 ppm ( $\Phi = 0.8$ )	1 ppm ( $\Phi = 0.8$ )
CO@15%O <sub>2</sub>	33 ppm ( $\Phi = 0.8$ )	289 ppm ( $\Phi = 0.8$ )	204 ppm ( $\Phi = 0.8$ )	35 ppm ( $\Phi = 0.8$ )

(continued on next page)

Table 2 (continued)

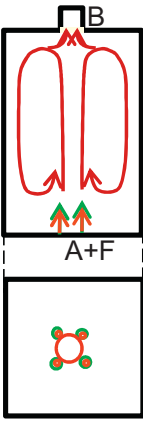
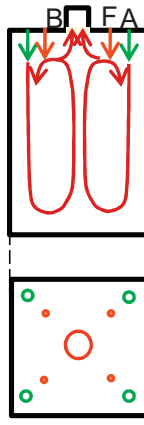
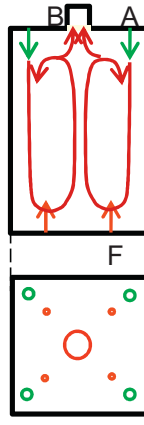
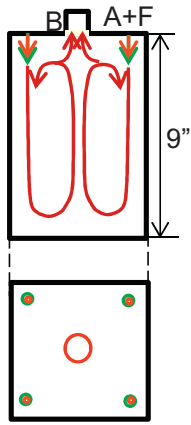
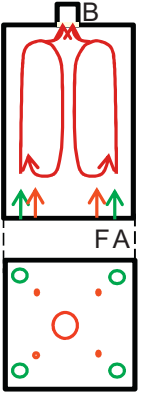
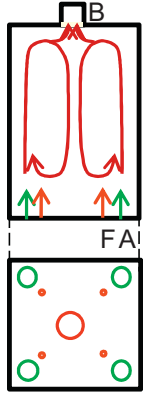
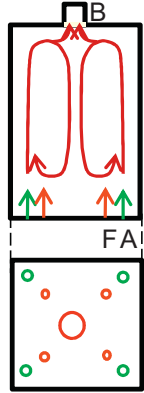
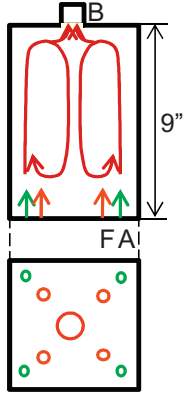
				
Configuration	(5) CDC, Gupta et al., UMD, 2010 FP	(6) CDC, Gupta et al., UMD, 2010 RS	(7) CDC, Gupta et al., UMD, 2010 RO	(8) CDC, Gupta et al., UMD, 2010 RP
Thermal intensity	5 MW/m <sup>3</sup> -atm	5 MW/m <sup>3</sup> -atm	5 MW/m <sup>3</sup> -atm	5 MW/m <sup>3</sup> -atm
Heat load	25 kW	25 kW	25 kW	25 kW
Fuel	Methane	Methane	Methane	Methane
Pressure	1 atm	1 atm	1 atm	1 atm
Air velocity	139 m/s	128 m/s	128 m/s	139 m/s
Fuel velocity	–	97 m/s	97 m/s	–
Air diameter	4.8 mm	4.8 mm	4.8 mm	4.8 mm
Fuel diameter	–	1.6 mm	1.6 mm	–
$\tau_{air}$ (D/U)	0.035 ms	0.038 ms	0.038 ms	0.035 ms
$\tau_{fuel}$ (D/U)	–	0.016 ms	0.016 ms	–
Air temperature	300 K	300 K	300 K	300 K
Fuel temperature	–	300 K	300 K	–
NO@15%O <sub>2</sub>	2 ppm ( $\Phi = 0.8$ )	11 ppm ( $\Phi = 0.8$ )	9 ppm ( $\Phi = 0.8$ )	1 ppm ( $\Phi = 0.8$ )
CO@15%O <sub>2</sub>	663 ppm ( $\Phi = 0.8$ )	208 ppm ( $\Phi = 0.8$ )	38 ppm ( $\Phi = 0.8$ )	5 ppm ( $\Phi = 0.8$ )
				
Configuration	(9) CDC, Gupta et al., UMD, 2010 FS1	(10) CDC, Gupta et al., UMD, 2010 FS1	(11) CDC, Gupta et al., UMD, 2010 FS1	(12) CDC, Gupta et al., UMD, 2010 FS1
Thermal intensity	5 MW/m <sup>3</sup> -atm	5 MW/m <sup>3</sup> -atm	5 MW/m <sup>3</sup> -atm	5 MW/m <sup>3</sup> -atm
Heat load	25 kW	25 kW	25 kW	25 kW
Fuel	Methane	Methane	Methane	Methane
Pressure	1 atm	1 atm	1 atm	1 atm
Air velocity	46 m/s	24 m/s	128 m/s	128 m/s
Fuel velocity	97 m/s	97 m/s	24 m/s	11 m/s
Air diameter	mm	mm	4.8 mm	4.8 mm
Fuel diameter	1.6 mm	1.6 mm	mm	–
$\tau_{air}$ (D/U)	0.173 ms	0.463 ms	0.038 ms	0.038 ms
$\tau_{fuel}$ (D/U)	0.016	0.016 ms	0.132 ms	0.433 ms
Air temperature	300 K	300 K	300 K	300 K
Fuel temperature	300 K	300 K	300 K	300 K
NO@15%O <sub>2</sub>	11 ppm ( $\Phi = 0.8$ )	15 ppm ( $\Phi = 0.8$ )	7 ppm ( $\Phi = 0.8$ )	8 ppm ( $\Phi = 0.8$ )
CO@15%O <sub>2</sub>	98 ppm ( $\Phi = 0.8$ )	145 ppm ( $\Phi = 0.8$ )	47 ppm ( $\Phi = 0.8$ )	70 ppm ( $\Phi = 0.8$ )



Table 2 (continued)

	(13) CDC, Gupta et al., UMD, 2011	(14) CDC, Gupta et al., UMD, 2011	(15) CDC, Gupta et al., UMD, 2011	(16) CDC, Gupta et al., UMD, 2011	(17) CDC, Gupta et al., UMD, 2011	
	Configuration	FS	FO	FP	RO	RP
Thermal intensity	28 MW/m <sup>3</sup> -atm	28 MW/m <sup>3</sup> -atm	28 MW/m <sup>3</sup> -atm	28 MW/m <sup>3</sup> -atm	28 MW/m <sup>3</sup> -atm	
Heat load	6.25 kW	6.25 kW	6.25 kW	6.25 kW	6.25 kW	
Fuel	Methane	Methane	Methane	Methane	Methane	
Pressure	1 atm	1 atm	1 atm	1 atm	1 atm	
Air velocity	146 m/s	146 m/s	157 m/s	146 m/s	157 m/s	
Fuel velocity	97 m/s	97 m/s	–	97 m/s	–	
Air diameter	4.8 mm	4.8 mm	4.8 mm	4.8 mm	4.8 mm	
Fuel diameter	1.6 mm	1.6 mm	–	1.6 mm	–	
$\tau_{air}$ (D/U)	0.033 ms	0.033 ms	0.031 ms	0.033 ms	0.031 ms	
$\tau_{fuel}$ (D/U)	0.016 ms	0.016 ms	–	0.016 ms	0.016 ms	
Air temperature	300 K	300 K	300 K	300 K	300 K	
Fuel temperature	300 K	300 K	–	300 K	–	
NO@15%O <sub>2</sub>	9 ppm ( $\Phi = 0.7$ )	9 ppm ( $\Phi = 0.7$ )	2 ppm ( $\Phi = 0.7$ )	12 ppm ( $\Phi = 0.7$ )	1 ppm ( $\Phi = 0.7$ )	
CO@15%O <sub>2</sub>	465 ppm ( $\Phi = 0.7$ )	250 ppm ( $\Phi = 0.7$ )	2282 ppm ( $\Phi = 0.7$ )	163 ppm ( $\Phi = 0.7$ )	64 ppm ( $\Phi = 0.7$ )	

	(18) CDC, Gupta et al., UMD, 2011	(19) CDC, Gupta et al., UMD, 2011	(20) CDC, Gupta et al., UMD, 2011
Configuration	FS	FS	FS
Thermal intensity	20 MW/m <sup>3</sup> -atm	30 MW/m <sup>3</sup> -atm	40 MW/m <sup>3</sup> -atm
Heat load	25 kW	25 kW	25 kW
Fuel	Methane	Methane	Methane
Pressure	1 atm	1 atm	1 atm
Air velocity	171 m/s	171 m/s	171 m/s
Fuel velocity	97 m/s	97 m/s	97 m/s
Air diameter	4.8 mm	4.8 mm	4.8 mm
Fuel diameter	1.6 mm	1.6 mm	1.6 mm
$\tau_{air}$ (D/U)	0.028 ms	0.028 ms	0.028 ms
$\tau_{fuel}$ (D/U)	0.016 ms	0.016 ms	0.016 ms
Air temperature	300 K	300 K	300 K
Fuel temperature	300 K	300 K	300 K
NO@15%O <sub>2</sub>	7 ppm ( $\Phi = 0.6$ )	8 ppm ( $\Phi = 0.6$ )	7 ppm ( $\Phi = 0.6$ )
CO@15%O <sub>2</sub>	19 ppm ( $\Phi = 0.6$ )	28 ppm ( $\Phi = 0.6$ )	48 ppm ( $\Phi = 0.6$ )

(continued on next page)

Table 2 (continued)

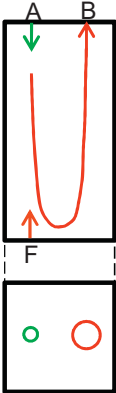
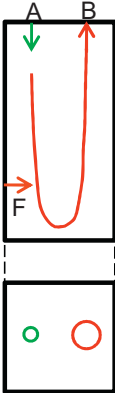
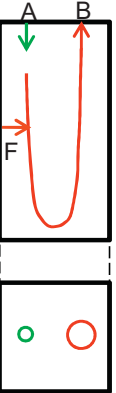
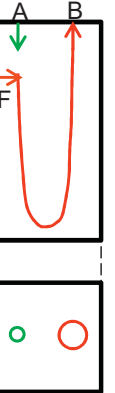
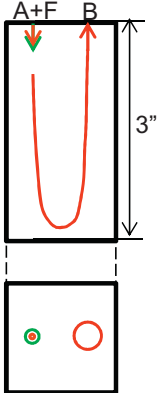
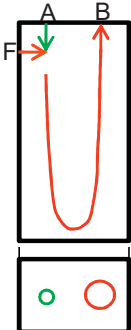
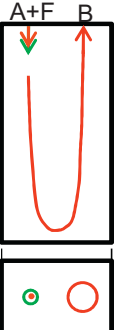
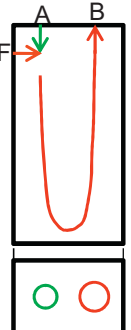
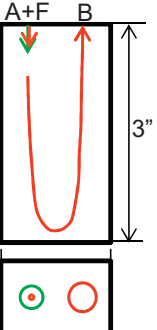
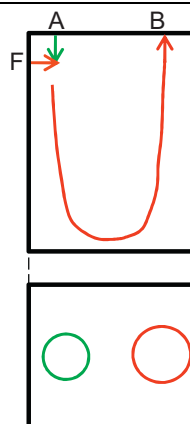
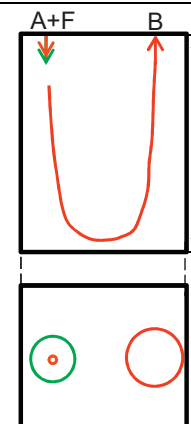
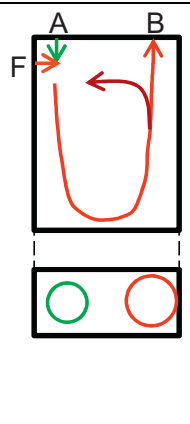
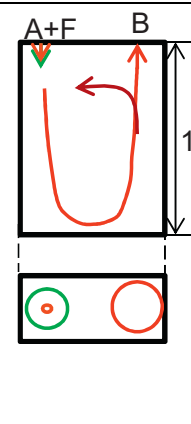
					
	(21) CDC, Gupta et al., UMD, 2011	(22) CDC, Gupta et al., UMD, 2011	(23) CDC, Gupta et al., UMD, 2011	(24) CDC, Gupta et al., UMD, 2011	(25) CDC, Gupta et al., UMD, 2011
Configuration	RO	RC	RC	RC	RP
Thermal intensity	57 MW/m <sup>3</sup> -atm	57 MW/m <sup>3</sup> -atm	57 MW/m <sup>3</sup> -atm	57 MW/m <sup>3</sup> -atm	57 MW/m <sup>3</sup> -atm
Heat load	6.25 kW	6.25 kW	6.25 kW	6.25 kW	6.25 kW
Fuel	Methane	Methane	Methane	Methane	Methane
Pressure	1 atm	1 atm	1 atm	1 atm	1 atm
Air velocity	146 m/s	146 m/s	146 m/s	146 m/s	157 m/s
Fuel velocity	97 m/s	97 m/s	97 m/s	97 m/s	–
Air diameter	4.8 mm	4.8 mm	4.8 mm	4.8 mm	4.8 mm
Fuel diameter	1.6 mm	1.6 mm	1.6 mm	1.6 mm	–
$\tau_{air}$ (D/U)	0.033 ms	0.033 ms	0.0338 ms	0.033 ms	0.031 ms
$\tau_{fuel}$ (D/U)	0.016 ms	0.016 ms	0.016 ms	0.016 ms	–
Air	temperature	300 K	300 K	300 K	300 K
300 K					
Fuel	temperature	300 K	300 K	300 K	300 K
–					
NO@15%O <sub>2</sub>	9 ppm ( $\Phi = 0.7$ )	6 ppm ( $\Phi = 0.7$ )	3 ppm ( $\Phi = 0.7$ )	3 ppm ( $\Phi = 0.7$ )	2 ppm ( $\Phi = 0.7$ )
CO@15%O <sub>2</sub>	202 ppm ( $\Phi = 0.7$ )	203 ppm ( $\Phi = 0.7$ )	131 ppm ( $\Phi = 0.7$ )	57 ppm ( $\Phi = 0.7$ )	96 ppm ( $\Phi = 0.7$ )
					
	(26) CDC, Gupta et al., UMD, 2012	(27) CDC, Gupta et al., UMD, 2012	(28) CDC, Gupta et al., UMD, 2012	(29) CDC, Gupta et al., UMD, 2012	
Configuration	RC	RP	RC	RP	
Thermal intensity	85 MW/m <sup>3</sup> -atm	85 MW/m <sup>3</sup> -atm	53 MW/m <sup>3</sup> -atm	53 MW/m <sup>3</sup> -atm	
Heat load	6.25 kW	6.25 kW	3.91 kW	3.91 kW	
Fuel	Methane	Methane	Methane	Methane	
Pressure	1 atm	1 atm	1 atm	1 atm	
Air velocity	146 m/s	157 m/s	92 m/s	97 m/s	
Fuel velocity	97 m/s	–	61 m/s	–	
Air diameter	4.8 mm	4.8 mm	7.9 mm	7.9 mm	
Fuel diameter	1.6 mm	–	1.6 mm	–	
$\tau_{air}$ (D/U)	0.033 ms	0.031 ms	0.086 ms	0.082 ms	
$\tau_{fuel}$ (D/U)	0.016 ms	–	0.016 ms	–	
Air temperature	300 K	300 K	600 K	600 K	
Fuel temperature	300 K	–	300 K	–	
NO@15%O <sub>2</sub>	4 ppm ( $\Phi = 0.7$ )	2 ppm ( $\Phi = 0.7$ )	4 ppm ( $\Phi = 0.5$ )	1 ppm ( $\Phi = 0.5$ )	
CO@15%O <sub>2</sub>	115 ppm ( $\Phi = 0.7$ )	65 ppm ( $\Phi = 0.7$ )	27 ppm ( $\Phi = 0.5$ )	34 ppm ( $\Phi = 0.5$ )	
Pressure loss	–	–	$\Delta P < 5\%$	$\Delta P < 5\%$	
Pressure fluctuations	–	–	$P_r$ ms < 0.025%	$P_r$ ms < 0.025%	

Table 2 (continued)

				
Configuration	(30) CDC, Gupta et al., UMD, 2012 RC	(31) CDC, Gupta et al., UMD, 2012 RP	(32) CDC, Gupta et al., UMD, 2013 RC	(33) CDC, Gupta et al., UMD, 2013 RP
Thermal intensity	170 MW/m <sup>3</sup> -atm	170 MW/m <sup>3</sup> -atm	340 MW/m <sup>3</sup> -atm	340 MW/m <sup>3</sup> -atm
Heat load	4.7 kW	4.7 kW	4.7 kW	4.7 kW
Fuel	Methane	Methane	Methane	Methane
Pressure	1 atm	1 atm	1 atm	1 atm
Air velocity	92 m/s	98 m/s	92 m/s	98 m/s
Fuel velocity	73 m/s	–	44 m/s	–
Air diameter	7.9 mm	7.9 mm	7.9 mm	7.9 mm
Fuel diameter	1.6 mm	–	2.4 mm	–
$\tau_{\text{air}}$ (D/U)	0.086 ms	0.081 ms	0.086 ms	0.081 ms
$\tau_{\text{fuel}}$ (D/U)	0.024 ms	–	0.054 ms	–
Air temperature	600 K	600 K	600 K	600 K
Fuel temperature	300 K	–	300 K	–
NO@15%O <sub>2</sub>	8 ppm ( $\Phi = 0.6$ )	3 ppm ( $\Phi = 0.6$ )	4 ppm ( $\Phi = 0.6$ )	2 ppm ( $\Phi = 0.6$ )
CO@15%O <sub>2</sub>	81 ppm ( $\Phi = 0.6$ )	102 ppm ( $\Phi = 0.6$ )	115 ppm ( $\Phi = 0.6$ )	85 ppm ( $\Phi = 0.6$ )
UHC@15%O <sub>2</sub>	–	–	<10 ppm ( $\Phi = 0.6$ )	<10 ppm ( $\Phi = 0.6$ )

## References

- [1] Weber R, Smart JP, vd Kamp W. On the (MILD) combustion of gaseous, liquid, and solid fuels in high temperature preheated air. *Proc Combust Inst* 2005;30:2623–9.
- [2] Colorado AF, Herrera BA, Amell AA. Performance of a flameless combustion furnace using biogas and natural gas. *Bioresour Technol* 2010;101:2443–9.
- [3] Tsuji H, Gupta AK, Hasegawa T, Katsuki M, Kishimoto K, Morita M. High temperature air combustion: from energy conservation to pollution reduction. CRC Press; 2003.
- [4] Wunning JA, Wunning JG. Flameless oxidation to reduce thermal NO<sub>x</sub> formation. *Prog Energy Combust Sci* 1997;23:81–94.
- [5] Sobiesiak A, Rahbar S, Becker HA. Performance characteristics of the novel low-NO<sub>x</sub> CGRI burner for use with high air preheat. *Combust Flame* 1998;115:93–125.
- [6] Dally BB, Riesmeier E, Peters N. Effect of fuel mixture on moderate and intense low oxygen dilution combustion. *Combust Flame* 2004;137:418–31.
- [7] Mi J, Li P, Dally BB, Craig RA. Importance of initial momentum rate and air-fuel premixing on moderate or intense low oxygen dilution (MILD) combustion in a recuperative furnace. *Energy Fuel* 2009;23:5349–56.
- [8] He Y. Flameless combustion of natural gas in the SJ/WJ furnace. PhD thesis-Queen's University; 2008.
- [9] Xing X, Wang B, Lin Q. Structure of reaction zone of normal temperature air flameless combustion in a 2 ton/h coal-fired boiler furnace. *J Power Energy* 2007;221:473–80.
- [10] Ozdemir IB, Peters N. Characteristics of the reaction zone in a combustor operating at mild combustion. *Exp Fluids* 2001;30:683–95.
- [11] Szego GC, Dally BB, Nathan GJ. Operational characteristics of a parallel jet MILD combustion burner system. *Combust Flame* 2009;156:429–38.
- [12] Yetter RA, Glassman I, Gabler HC. Asymmetric whirl combustion: a new low NO<sub>x</sub> approach. *Proc Combust Inst* 2000;28:1265–72.
- [13] Kumar S, Paul PJ, Mukunda HS. Studies on a high-intensity low-emission burner. *Proc Combust Inst* 2002;29:1131–7.
- [14] Kumar S, Paul PJ, Mukunda HS. Investigations of the scaling criteria for a mild combustion burner. *Proc Combust Inst* 2005;30:2613–21.
- [15] Vandervort CL. 9 ppm NO<sub>x</sub>/CO combustion system for “F” class industrial gas turbines. *J Eng Gas Turb Power* 2001;123:317–21.
- [16] Luckerath R, Meier W, Aigner M. FLOX<sup>®</sup> combustion at high pressure with different fuel compositions. *J Eng Gas Turb Power* 2008;130:011505-1–5-7.
- [17] Bobba MK, Gopalakrishnan P, Periagaram K, Seitzman JM. Flame structure and stabilization mechanisms in a stagnation-point reverse-flow combustor. *J Eng Gas Turb Power* 2008;130:031505.
- [18] Straub DL, Casleton KH, Lewis RE, Sidwell TG, Maloney DJ, Richards GA. Assessment of rich-burn, quick-mix, lean-burn trapped vortex combustor for stationary gas turbines. *J Eng Gas Turb Power* 2005;127:36–41.
- [19] Melo MJ, Sousa JMM, Costa M, Levy Y. Experimental investigation of a novel combustor model for gas turbines. *J Propul Power* 2009;25:609–17.
- [20] Vincent ET. The theory and design of gas turbines and jet engines. 1st ed. McGraw-Hill Book Co; 1950.
- [21] Shuman TR. NO<sub>x</sub> and CO formation for lean-premixed methane-air combustion in a jet-stirred reactor operated at elevated pressure. PhD thesis-University of Washington; 2000.
- [22] Hsu KY, Goss LP, Roquemore WM. Characteristics of a trapped-vortex combustor. *J Propul Power* 1998;14:57–65.
- [23] Verissimo AS, Rocha AMA, Costa M. Operational, combustion and emission characteristics of a small scale combustor. *Energy Fuels* 2011;25:2469–80.
- [24] Arghode VK, Gupta AK. Effect of flow field for colorless distributed combustion (CDC) for gas turbine combustion. *Appl Energy* 2010;87:1631–40.
- [25] Arghode VK, Gupta AK. Development of high intensity CDC combustor for gas turbine engines. *Appl Energy* 2011;88:963–73.
- [26] Arghode VK, Gupta AK. Investigation of forward flow distributed combustion for gas turbine application. *Appl Energy* 2011;88:29–40.
- [27] Arghode VK, Gupta AK. Investigation of reverse flow distributed combustion for gas turbine application. *Appl Energy* 2011;88:1096–104.
- [28] Arghode VK, Gupta AK. Hydrogen addition effects on methane-air colorless distributed combustion flames. *Int J Hydrogen Energy* 2011;36:6292–302.
- [29] Khalil AEE, Gupta AK. Swirling distributed combustion for clean energy conversion in gas turbine applications. *Appl Energy* 2011;88:3685–93.
- [30] Khalil AEE, Gupta AK. Distributed swirl combustion for gas turbine application. *Appl Energy* 2011;88:4898–907.
- [31] Arghode VK, Gupta AK, Bryden KM. High intensity colorless distributed combustion for ultra low emissions and enhanced performance. *Appl Energy* 2012;92:822–30.
- [32] Arghode VK, Khalil AEE, Gupta AK. Fuel dilution and liquid fuel operational effects on ultra-high thermal intensity distributed combustor. *Appl Energy* 2012;95:132–8.
- [33] Arghode VK, Khalil AEE, Gupta AK. Novel mixing for ultra-high thermal intensity distributed combustion. *Appl Energy* 2013;105:327–34.

- [34] Gupta AK. Thermal characteristics of gaseous fuel flames using high temperature air. *J Eng Gas Turbin Power* 2004;126:9–19.
- [35] Gupta AK, Bolz S, Hasegawa T. Effect of air preheat temperature and oxygen concentration on flame structure and emission. *J Energy Resour Technol* 1999;121:209–16.
- [36] Smith GP, Golden DM, Frenklach M, Moriarty NW, Eiteneer B, Goldenberg M, et al. <[http://www.me.berkeley.edu/gri\\_mech/](http://www.me.berkeley.edu/gri_mech/)>.
- [37] Shih T-H, Liou WW, Shabbir A, Yang Z, Zhu J. A new  $k-\varepsilon$  Eddy viscosity model for high reynolds number turbulent flows. *Comput Fluids* 1995; 24: 227–38.
- [38] Ricou FP, Spalding DB. Measurements of entrainment by axisymmetrical turbulent jets. *J Fluid Mech* 1961;11:21–32.
- [39] Li SC, Williams FA. Reaction mechanisms for methane ignition. *J Eng Gas Turbin Power* 2002;124:471–80.